Curvature-Density Functional Theory of Shape Transformation in Vesicles of Two-Component Lipid Systems

By

Ian MacKay

ABSTRACT

The shape transformations and composition variation of two-component model lipid membrane isolated vesicles are studied. These are studied as aggregates in low concentration solutions so that the vesicles are isolated from each other and interaction effects can be ignored. The seminal work of Julicher and Lipowsky derived a curvature-functional free energy, which has predicted or verified many of the experimentally observed behaviors of model vesicles. One aspect that has not been well explored is the composition variation of the liquid domains. In this work, the theory of Julicher and Lipowsky is modified to include couplings between the curvature and composition but the shape of the vesicle is restricted to include only ellipsoids of varying degree of eccentricity and constant area. We also introduce a free energy to describe bilayered micelles ("bicelles"). The energetics of this structure is studied and phase diagrams are found for various vesicle-bicelle transitions. The properties of liquid domains, including compositional variations with temperature are also discussed. These results are then compared to experiments on vesicles and bicelles using small angle neutron scattering and nuclear magnetic resonance.

NOTICE:
The author has granted a non-exclusive license allowing Library and Archives Canada to reproduce, publish, archive, preserve, conserve, communicate to the public by telecommunication or on the Internet, loan, distribute and sell theses worldwide, for commercial or non-commercial purposes, in microform, paper, electronic and/or any other formats.

The author retains copyright ownership and moral rights in this thesis. Neither the thesis nor substantial extracts from it may be printed or otherwise reproduced without the author's permission.

AVIS:
L'auteur a accordé une licence non exclusive permettant à la Bibliothèque et Archives Canada de reproduire, publier, archiver, sauvegarder, conserver, transmettre au public par télécommunication ou par l'Internet, prêter, distribuer et vendre des thèses partout dans le monde, à des fins commerciales ou autres, sur support microforme, papier, électronique et/ou autres formats.

L'auteur conserve la propriété du droit d'auteur et des droits moraux qui protège cette thèse. Ni la thèse ni des extraits substantiels de celle-ci ne doivent être imprimés ou autrement reproduits sans son autorisation.

In compliance with the Canadian Privacy Act some supporting forms may have been removed from this thesis.

While these forms may be included in the document page count, their removal does not represent any loss of content from the thesis.

Conformément à la loi canadienne sur la protection de la vie privée, quelques formulaires secondaires ont été enlevés de cette thèse.

Bien que ces formulaires aient inclus dans la pagination, il n'y aura aucun contenu manquant.

Canada

Table of Contents

1. INTRODUCTION

1.1. One Component Membrane Systems

Lipids are one of the principle components of biological membranes forming a selectively permeable barrier between the cell's inner and outer environments. The phospholipid molecule is a surfactant (surface active agent) that consists of a glycerine hinge that connects a phosphatic head group (which perhaps may be very complex) and a tail group of two fatty acid tails which are typically about 15-18 carbons long (see figure 1.1).

Fig1.1. Diagram of a phospholipid molecule

Often, one tail is longer than the other and they may be saturated differently (Peliti, 1997a) but in most of the experiments relevant to this project, they are identical (for example, DMPC-dimyristolphosphatidylcholine and DHPC-dihexanoylphosphaticdylcholine). The phosphatic head, polarized or charged, attracts water molecules and is thus strongly hydrophilic; the fatty acid tails are non-polar and are less attracted to water than the head. Thus, they are relatively hydrophobic. Because of these two simultaneous properties of the surfactant, it is also called an "amphiphile" (loving both polar and non-polar molecules).

In amphiphilic solution, phospholipids undergo a structural transformation and arrange into complex structures called micelles that shield their tails from water, leaving their polar heads exposed to water. They form when the phospholipid concentration is above a threshold value commonly called the critical micelle concentration, or CMC for

short. Above this concentration, even though micelles are formed, there is still a small number of monomers in solution. The CMC has an exponential dependence on the hydrophobic area of the tail group and ranges from about 10^{-5} molar for an eight carbon chain double tail PC to 10^{-10} for a sixteen carbon chain double tail PC (Boal, 2002a).

Depending on molecular geometry, amphiphiles will form various micelle shapes such that amphiphiles are closed packed and their hydrocarbon chains are shielded from water (Boal, 2002b) as depicted in figure 1.2.
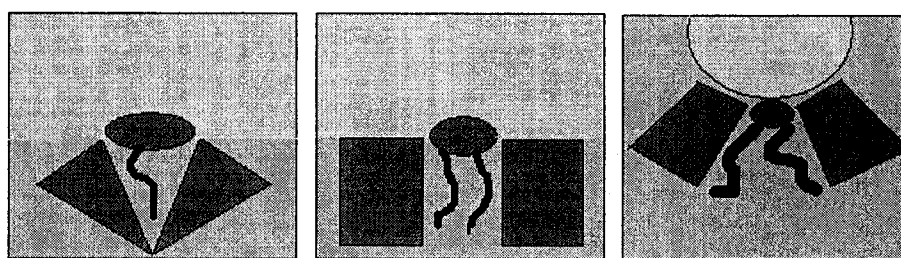
Fig1.2. The relation of interface shape to molecular geometry. (a) Single chains tend to form micelles. (b) dual chain phospholipids with moderate size head groups prefer bilayers. (c) Phospholipids with small head groups tend to form inverted micelles

A parameter that characterizes the molecular geometry is the shape factor, which is given by $v_{hc}/(a_0 l_{hc})$ where v_{hc} is the volume of the hydrocarbon chain, a_0 is the average membrane surface area of the molecule and l_{hc} is the projected length of the hydrocarbon chain. The shape factor is roughly the ratio of the volume of the hydrocarbon chain volume over the head group volume. For a shape factor less than 1/3, the amphiphiles tend to form spherical micelles as shown in part a) of figure 1.3:
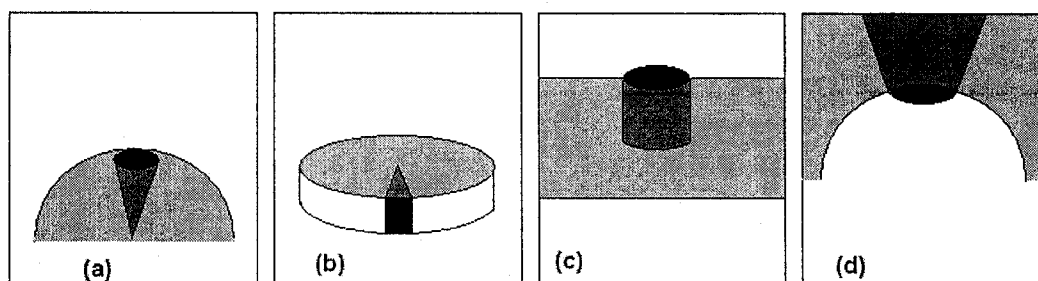
Fig1.3. Packing constraints experienced by a typical amphiphile in four aggregates: (a) spherical micelle, (b) cylindrical micelle, (c) bilayer, and (d) inverted micelle. The cross sectional area is coloured black while the molecular shape is gray.

Such amphiphiles are characterized by a large headgroup area a_0 compared to v_{hc}/l_{hc} corresponding to the conical shape also shown in the figure.

For shape factors between 1/3 and ½, the amphiphiles are more wedged shaped and the aggregates tend to be more cylindrical shaped, as in figure 1.3b). When the shape factor is greater than ½ but less than unity, the molecule has more of a cylindrical geometry, with the ideal cylinder corresponding to a shape factor of unity, and sheet-like lamellar bilayers as in figure 1.3c) have the optimal closed-packed structure. The bilayers are comprised of two monolayers stacked so that the lipid tails are in the interior. The value of a_0 for phospholipids is typically 0.5 nm^2 which is about double the average cross-sectional area of a single hydrocarbon chain. Therefore dual chain phospholipids, ideal for biological membranes, will have a shape factor of around unity, forming bilayers. The bilayer structure is shown in figure 1.4.
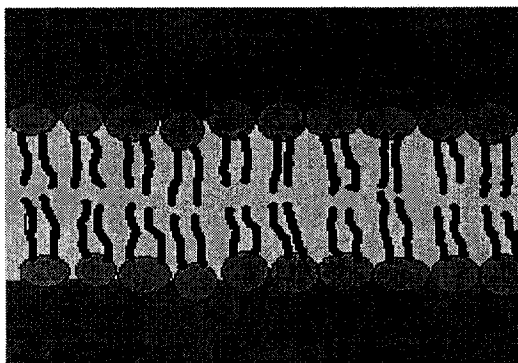
Fig 1.4. The lipid bilayer structure of dual-chain lipid molecules separating two aqueous domains.

For shape factors greater than 1 we have the hydrocarbon volume being larger than the product of the head group area with the chain length. With a relatively small head

group, the molecules have the truncated cone shape and form inverted micelles which is shown in figure 1.3d).

We have seen that micelles form at the CMC, but at this concentration the micelles themselves do not have long range order. Above the CMC micelles will interact with each other when the concentration is large enough. The inter-micelle forces include excluded volume interactions and steric interactions which are repulsive. When the concentration of amphiphile is increased, repulsive interactions between the micelles become significant and this repulsion leads to crystallization of the micelles into a structure with long-range order (Jones, 2002a). Some these phases are shown in the figure 1.5:

(a)   (b)   (c)
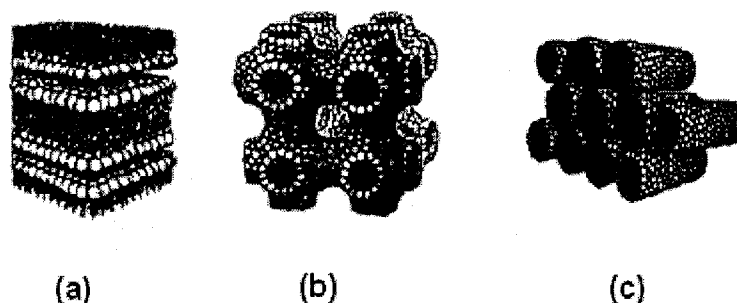
Fig 1.5. Some high concentration phases. (a) A section of the lamellar phase, (b) Plumber's nightmare, a bicontinuous phase and (c) cylindrical rods in a hexagonal phase. (From Jones, R. A. L., "Soft Condensed Matter", p148)

The phase behavior of these high concentration structures is very rich and well studied. We are interested in the behaviour of bilayered vesicle aggregates at concentrations above the CMC, but below the high concentration regime where interaction effects can be ignored and the vesicles can be considered isolated.

1.2.   One Component Bilayers and Model Vesicles

For systems of one kind of phospholipid in aqueous solutions, at sufficiently high

concentration, two-dimensional bilayer sheets are stable. These bilayer sheets are about

40Å-100Å in thickness and can be infinite in extent (Jones, 2002b). The edges of this

sheet are where the exposed hydrophilic hydrocarbon tails are located (see figure 1.6).

Because of this unfavourable arrangement, the exposed edge increases the energy of the

system (Boal, 2000).
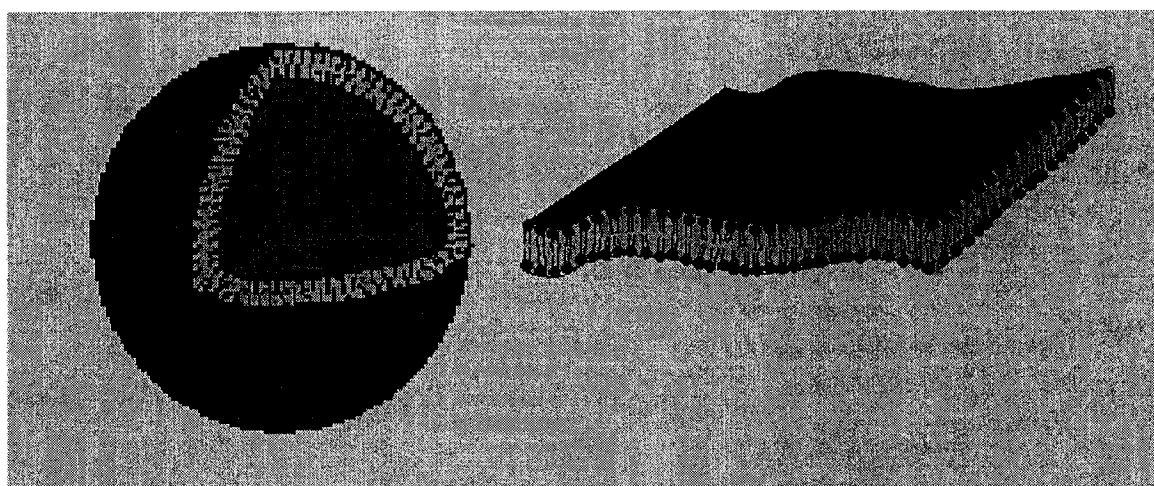
Fig 1.6. Cross section of a unilamellar vesicle (left). The bilayer sheet structure (right)

However, if the edges of the sheet are allowed to close up on one another to give a

closed unilamellar vesicle as in figure 1.6, the extra edge energy may be eliminated. But

to allow the bilayer sheet to close up requires the bilayer to bend which also requires

additional energy, called the curvature energy. The curvature energy will be discussed in

section 2.2.3. The curvature energy needs to be set against the energy decrease from

eliminating the edge, together with the gain in translational entropy that arises from going

from an infinite lamellar sheet system with small polydispersity to a finite vesicle system

with much larger polydispersity (Jones, 2002b).

At concentration significantly above the CMC the bilayers are stacked, giving rise to the lamellar phase depicted in figure 1.5a). This is a phase with one-dimensional long–range order in the direction normal to the bilayer.

For one component systems, vesicles are generally not stable. Sheet-like aggregates are more stable because of the symmetric bilayer which has no curvature preference. However, vesicles can be obtained in the lab relatively easily by using ultrasound to break up the bilayer in the lamellar phase (Benton, 1987). These sonicated vesicles are only metastable but are reasonably long-lived on experimental timescales (Jones, 2002b).

The radius of unilamellar vesicles (ULV's) is commonly between 10 and 100 nm (Nieh, 2003). In experiments, one has a solution containing many of these ULVs whose sizes may be polydispers or monodisperse (Nieh, 2003) which gives rise to a translational entropy of the system. But, in many theoretical studies (including this one) the entropic contribution to the free energy due to polydispersity are neglected since it is the dynamics of only a single vesicle that are studied (Safran *et al.*, 1991; Julicher and Lipowski, 1996).

1.3. Vesicles in Biological Systems

For a typical biological membrane, the lateral diffusion coefficient is around 1 $\mu m^2 s^{-1}$, so a molecule can move from one end of a vesicle to the other in about one second. However, it takes about a few hours for molecule to skip from one monolayer to the other which is of the same order of magnitude as the characteristic time to exchange with the solution. Therefore, on small time scales one can think of the phospholipids molecules as being bound to one layer but free to diffuse laterally in it (Peliti, 1997a).

Vesicles are of great importance in the pharmaceutical industry. For example, they are used to encapsulate drug molecules during delivery to a target part of the living system. This protects the molecule from unwanted interactions. If the vesicle breaks up in a controlled way at the target, then the drug can be delivered efficiently. Vesicles are also commonly thought of as a simple model of a biological cell, whose contents are separated from the outside world by the phospholipid membrane (Jones, 2002b).

1.4. Two Component Systems/Phase Formation

Living membranes are usually comprised of two or more kinds of lipids, as well as cholesterol and proteins. On the inside of the membrane is the cytoskeleton which consists of a net of proteic filaments anchored to the membrane via protein complexes (Peliti, 1997a). Experiments on bio-membranes usually neglect the cytoskeleton, and focus on two-lipid systems with or without the addition of cholesterol (Nieh, et al., 2005; Baumgart, Hess, Webb, 2003; Triba et al., 2005; Veatch, Keller, 2005).

Of the many studies of two component vesicles, the theoretical study of vesicle budding induced by the presence of domains is of particular interest. In that study the domain itself, which is composed of a lipid with higher curvature than the bulk, forms a small bud off the main vesicle (Julicher and Lipowski, 1993). In those systems, there is an extra energy term due to the presence of the domain boundary. This edge energy, which is proportional to the length of the edge, competes with the bending energy of the vesicle. The domain can form a high curvature bud by decreasing the length of the domain edge, which lowers the edge energy. If the energy loss due to the decreasing

domain edge is greater than the bending energy gain of the high curvature bud, then the budded state will be stable.

These domains are also studied as models of lipid rafts, which are small (< 100 nm) inhomogeneous regions of lipids and membrane-bound proteins found in cell plasma membranes. These rafts are associated with membrane signaling pathways and have recently generated interest among cell biology and membrane biophysics researchers (Veatch and Keller, 2005).

It was mentioned in section 1.2 that in a one-component bilayer system the lamellar phase is generally more stable than the vesicle phase (except at extremely low concentrations, of course). This is due to the energy gain of bending the bilayer. The bending energy is minimum for a symmetric bilayer that is flat (zero curvature) leading to a vanishing spontaneous curvature. However, if there are two components, the local bilayer composition may be distributed in a non-symmetric way and thus the local spontaneous curvature would be non-zero (Safran et al., 1991). The implication of this is that for two-component systems we can have stable vesicles, which does not happen in one-component systems. Stable two-component vesicles have been observed in numerous experiments (Baumgart, Hess, Webb 2003; Neih et al., 2005; Triba et al. 2005).

1.5. The Bicelle Phase

Another structure consisting of the phospholipid bilayer is the bilayered micelle also called the "bicelle", which is shown in figure 1.7:
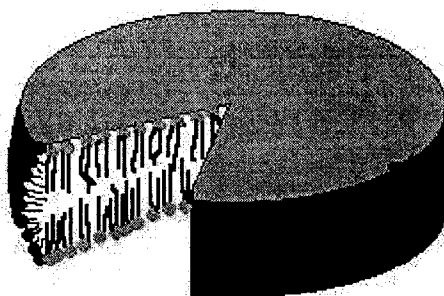
Fig 1.7. The bilayered micelle, also known as the bicelle structure. The long chain molecules (in green) are situated on the major faces of the bicelle. The short chain molecules occupy the rim.

Bicelles are recognized as potentially important magnetically alignable substrates for solid-state nuclear magnetic resonance and neutron scattering studies of membrane-associated peptides and proteins (Katsaras *et al.*, 1997; Sanders *et al.*, 1992; Hare *et al.*, 1995; Neih *et al.*, 2001; Neih *et al.*, 2002). They are composed of short-tail and long-tail phospholipids with the short tail lipids situated to form a high curvature rim along the side of the bicelle and the long tail contained in the bilayer as in figure 1.7. This structure has been inferred from small angle neutron scattering experiments (Nieh *et al.*, 2005; Nieh *et al.*, 2003) and nuclear magnetic resonance experiments (Triba *et al.*, 2005; Andersson and Maler, 2006) which have used bicelles made of DMPC and DHPC. They exist in experiments with a radius typically between 10 and 100 nm and a thickness generally between 4 and 5 nm (Nieh *et al.*, 2005; Boal, 2000).

The bicelles also have an additional feature in that they possess an edge energy associated with the discontinuity at the edge of the disk as can be seen from figure 1.7. The energy penalty for the formation of edges can be characterized by an edge tension, an energy per unit length along the edge of the bicelle. Due to the edge energy the bicelle disk is circular, since this is the configuration that minimizes the edge perimeter for a given volume.

Using theoretical models, Boal and Raudino independently proposed the existence of bicelles in one-component phospholipids systems (Boal, 2000; Raudino, 1995). However, its edge consists of the exposed tails of the bilayer and does not have phospholipids rounding out the edges (see figure 1.8).
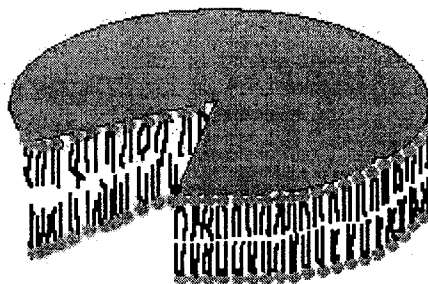
Fig 1.8. One component bicelle

The unfavourable configuration of the exposed hydrophobic tails gives rise to an edge energy in much the same way that the high curvature edge does in the two component structure. However, the edge energy would be greater for the one-component bicelles. To describe the hydrophobic energy due to the exposed tails, one can use, to simplest approximation, the same form of the free energy functional as the two component bicelle disk described earlier. Microscopically, the two structures have different interactions, but phenomenologically the edge energy can be described by the same parameter in the macroscopic sense.

1.6. Experiments Involving Bicelles

There have been many experimental studies over the years that have examined the transitions between bicelles, vesicles and lamellar phases. In the experiments to be discussed, the systems are at low enough concentration such that the aggregates do not interact and crystallization of the micelles does not occur. The systems under study are

generally two-component systems of short-tail and long-tail phospholipids. DHPC (two 6-carbon-long saturated acyl chains) and DMPC (two 14-carbon-long saturated hydrocarbon chain, no double bonds) are usually used. Sometimes DMPG (dimyristol-phosphatidyglycerol) is substituted for DMPC because it is useful for stabilizing bilayer systems (Losonczi and Prestegard, 1998). It differs from DMPC only by its anionic head group.

In the small angle neutron scattering (SANS) experiments, it has been observed that for a relatively high concentration, as the temperature is raised, the bicelles coalesce to form lamellar bilayers that happen to have hole defects littered along the surface. It is inferred that these holes themselves are lined with DHPC along their edges (Nieh *et al.*, 2005). This result can be understood by considering that the edge of the bicelle is an unfavourable high curvature configuration and thus gives rise to an effective edge energy as described in the last section. Therefore, the edge to area ratio of the bicelles will tend to be minimized, which is facilitated by their coalescence. Upon dilution, the lamellar bilayers undergo an unbinding transition at a critical concentration and form polydisperse unilamellar vesicles (ULV's).

Another study used mixtures of DMPC/DHPC and DMPC/DHPC/DMPG doped with Tm^{3+} ions (to facilitate bilayer alignment in the presence of an applied magnetic field) and observed that bilayers formed for low temperatures. At high temperature and concentration, stacks of lamellae with pores whose edges are lined with short chain DHPC are formed. For lower concentrations, unilamellar vesicles exist, while at intermediate concentrations the ULV's coexist with the lamellar phase. The phase diagram for this phase behavior is given in figure 1.9 (Nieh *et al.* 2001):
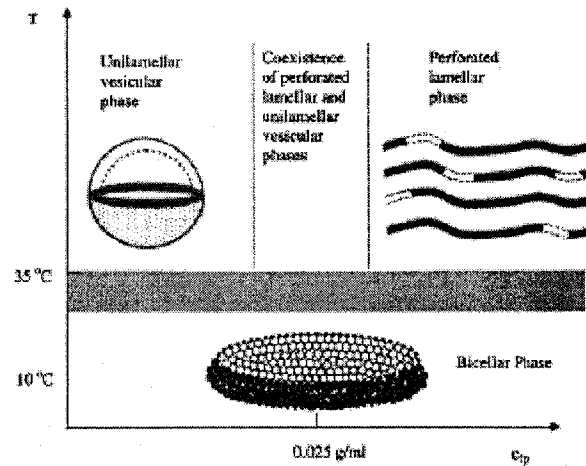
Fig 1.9. Schematic of the phase diagram determined by Nieh et al. showing the phase behavior of vesicular, bicellar , and lamellar phases. The phase transition temperature is at 35° C.

Nuclear Magnetic Resonance (NMR) experiments have also been done on

DMPC/DHPC systems. One study suggests that the segregation of DHPC on the rim and

DMPC on the bilayer is not always complete (Triba *et al.*, 2005). As the temperature is

raised above the gel-liquid crystal transition temperature, T_m, of DMPC the two

components begin to mix. Above T_m there is a small fraction of DHPC in the DMPC rich

area and vice versa. While some investigators have suggested that the observed

measurements are accounted for by an increase of the short-tail DHPC molecules in the

solution, this does not account for some of the observed structures and the inter-bicelle

two-component mixing model explains the structures more accurately. It is also found

that this fraction of mixing increases slightly in this pseudobinary system as temperature

increases above the transition temperature, T_m, and that the molar fraction, ε, of DHPC in

the DMPC-rich bilayer section is, to first approximation, only temperature dependent.

The temperature dependence of ε is given in figure 1.10 (Triba *et al.* 2005).
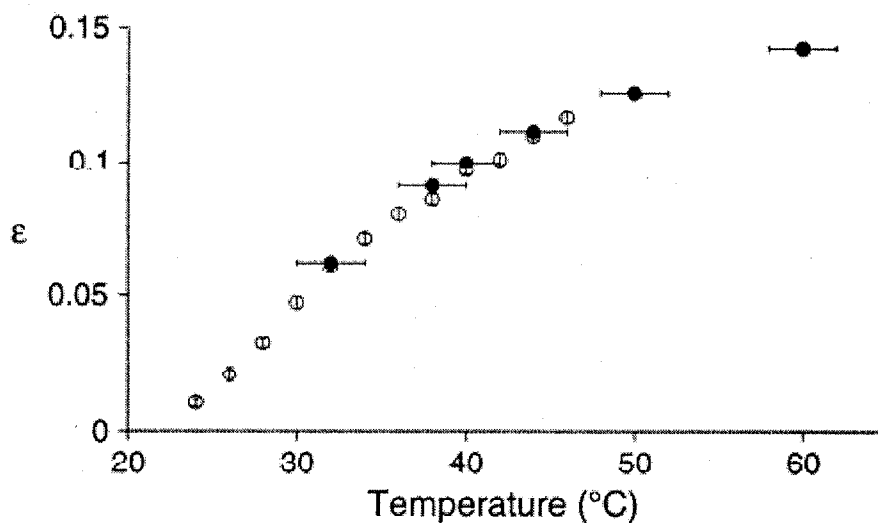
Fig 1.10. Molar fraction ε of lipids with a short chain (DHPC) in the bilayer section as a function of temperature. The black circles and the white circles represents two different methods used by the authors of the study (see Triba et al. 2005)

The NMR study by Triba *et al.* also describes a possible mechanism for a bicelle-vesicle transition that occurs at high temperatures, which is given by the following: As the temperature is increased above T_v, a new transition is observed by NMR and is accompanied by a modification of the macroscopic characteristics of the sample, which become milky and fluid. The ε increase remains small (figure 1.10) yet it theoretically initiates a rapid divergence of the bicelle radius for a critical value of ε:

$$\varepsilon_{lim} = \frac{1}{q+1}$$

(1.1)

where q is the mol ratio of DMPC/DHPC. The explanation for this divergence is based on the geometry of the bicelle. The bilayer edge increases as R, while the area increases like R^2. Above a critical value of ε, the increased DHPC partition into the bilayer section of the disks does not leave enough short-chain lipids to stabilize the edges. The edge energy is also increased from the growth in edge length. Therefore, in order to reduce the exposed edges, the bilayers must either fuse together to make large size lamellae or reseal

by forming bilayered vesicles. If large lamellae are formed, their bending modulus may be reduced by the mixing of the two components in the bilayer and the high temperature of the sample may facilitate undulation and, eventually, the spontaneous resealing of the bilayer to form a vesicle.

A tentative phase diagram for bicelles and vesicles produced by this experimental study with an accompanying description is given in figure 1.11. The following diagram is incomplete, however. The regions of dotted lines represent extrapolations by the authors where the precise boundary of the domains has not been measured.
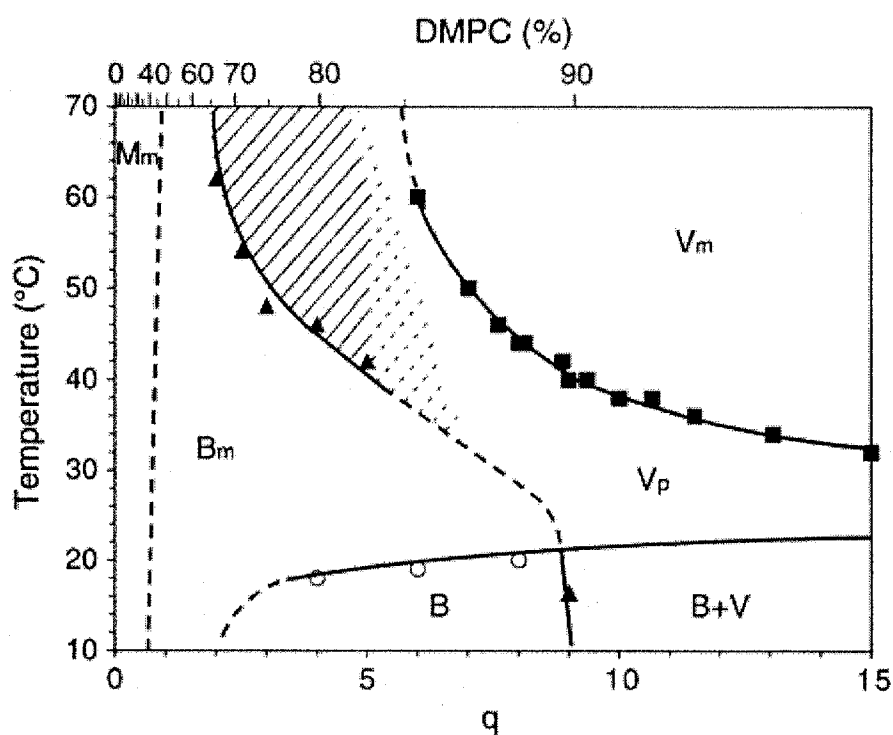
Fig 1.11. Tentative temperature/composition diagram of DMPC/DHPC mixtures, at a concentration in water of 25% (w/w). q represents the mole ratio of DMPC/DHPC. The dotted lines represent incomplete regions. (from Triba et al. 2005)

The boundary indicated by open circles, corresponds to a transition between bicelles with almost perfect segregation to bicelles with mixing between the DMPC and DHPC regions. The region labeled *B+V* corresponds to a co-existence region, where bicelles and vesicles

are equally stable. Full triangles correspond to a boundary between mixed bicelles and multilamellar vesicles, starting with perforated vesicles (V_p), coexisting with remaining mixed bicelles (*shaded zone*). The perforated vesicles have short chain DHPC lining the holes. Full squares correspond to a boundary between perforated vesicles and non-perforated vesicles whose bilayer consists of mixed DMPC and DHPC.

A possibility not mentioned by Triba *et al.* is that the dotted line between V_p and B_m may represent regions of B_m and V_p in co-existence.

1.7. Detection of the Oblate Structure

Another interesting structure is that of the oblate shaped vesicle, which was also observed in the SANS experiments (Nieh *et al.*, 2005) and is given in figure 1.12.
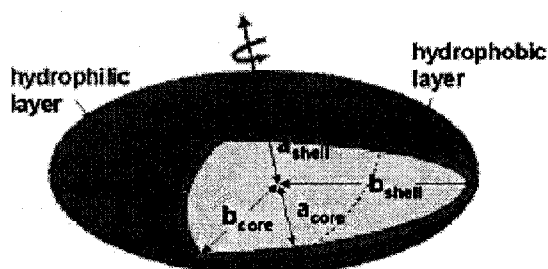
Fig 1.12. Oblate ellipsoid. a_{shell}, b_{shell}, a_{core} and b_{core} correspond to the various minor and major axes radii of the oblate ellipsoid's shell and core, repectively.

For low sample concentration (0.1 wt%), relative concentration of about ([DMPC]+[DMPG])/[DHPC] = 3.2, and very small amount of DMPG ([DMPG]/[DMPC] = 0.01), the sample was prepared at 10°C. The sample begins in the bicelle phase and upon heating forms small polydisperse unilamellar vesicles (ULV) with radius of 98Å. When the sample is cooled back to 10°C, the SANS data does not show the characteristic pattern for bicelles but instead a scattering curve best fit using monodisperse core-shell

oblate ellipsoids with major and minor radii of 180Å and 62Å, respectively. Reheating the sample gives a scattering curve identical to the initial one formed by the ULV, indicating that the ULV has conserved its size and mass. Theoretical calculations for the shell thickness give an increase of shell thickness from 36Å (ULV) to 45Å (oblate ellipsoids) and this increase in shell thickness is consistent with a bilayer undergoing a transition from the liquid crystal to gel phase. Furthermore, the measurements indicate that the size of the oblate and spherical vesicles are nearly the same.

The authors describe the oblate morphology in terms of the nascent stages of segregation between the gel-phase DMPC and DMPG from liquid crystal DHPC. The long chain lipids form a rigid planar structure which decreases the curvature energy resulting from the high bilayer bending rigidity as the temperature is decreased below the liquid crystal/gel transition temperature. However, since DHPC has a very high CMC, at this low concentration, there may be an insufficient amount of DHPC to stabilize the bicelle's rim. Therefore, the long chain planar bilayers are bridged via the flexible DHPC molecules, resulting in oblate ellipsoids.

1.8. The Relevance of a Composition-Curvature Theory

It was mentioned in section 1.4 that the study of two-component systems and their phase separation is important for understanding certain mechanisms for bud formation and for the study of lipid rafts. However, in the case of domain induced budding, the authors (Julicher and Lipowski, 1993) assume that highly segregated, homogenous, domains have already formed and that there is a discontinuous change in composition between them. This assumption, however, neglects that in general the amount of mixing

(the composition) varies continuously along the surface and that domain boundaries are not necessarily sharp but can be smooth. Then they construct the vesicle free energy of mixing in terms of the two separated domains plus a domain boundary energy as follows:

$$F_m = A^{(\alpha)} f^{(\alpha)} + A^{(\beta)} f^{(\beta)} + F_l \tag{1.2}$$

where the first term accounts for the mixing energy of one domain, the second term for the other domain, and the final term describes the energy due to the line tension between the two domains. The mixing energy is combined with the bending energy to examine vesicle stability. While this approach has predicted or verified many of the observed experimental behaviors, the authors neglect important factors that arise from the variation of local mixing. These factors include the entropy of mixing, and the change in the local bending rigidity and spontaneous curvature.

To investigate this, we will modify the approach of Julicher and Lipowsky and introduce a composition-curvature free energy functional that varies with the local composition and curvature. By performing functional minimization we obtain the equilibrium shape of the vesicle as well as the composition variation across the vesicle. To study bicelles we will introduce a bicelle edge energy term to the free energy functional. This will mimic the increase in energy at the bicelle's edge when short-chain lipids mix with long chain lipids (Triba *et al.*, 2005). Phase diagrams are obtained by standard statistical mechanical methods, and the results are compared to experimental diagrams of figures 1.9 and 1.11.

2. THEORY AND METHODS

2.1. Introduction

In this chapter, the free energy of the vesicle and the bicelle will be derived. There are a few terms that contribute to the total free energy of the system that have to be considered. The curvature or bending energy takes into account the bending energy of the bilayer, while the coupling energy takes into account the interaction between different pairs of molecules. The coupling energy is a result of the free energy of mixing that arises from the aforementioned generalization of the free energy of Julicher and Lipowski. The other terms that contribute to the free energy are the entropy of mixing, the chemical potential and the edge energy for the bicelle. With the full description of the free energy, Lagrange's principle of least action will be applied to the free energy functional, giving the self-consistent equation for the local composition. This will be used to obtain the stable vesicle shapes and the composition profile.

2.2. Introduction to Curvature

To describe the bending energy, it is necessary to introduce the curvature (Peliti, 1997b), which quantifies the amount of bending at a given point on the surface. One chooses the origin of a coordinate axes (x^1, x^2, x^3) to coincide with a point P while the direction is defined such that the first two coordinate axes are in the tangent plane and the third axes is orthogonal to it and directed toward the exterior. The shape of the membrane is given by a form called the *Monge representation* of the surface, given as follows:

$$x^3 = u\left(x^1, x^2\right) \tag{2.1}$$

Close to P, the function $u(x^1, x^1)$ will approximately be represented by the following quadratic form:

$$u\left(x^1, x^2\right) = \frac{1}{2} \sum_{i,j=1}^{2} \Omega_{ij} x^i x^j$$

Ω_{ij} is the curvature tensor. It has the eigenvalues c_1 and c_2, which are the two principal curvatures and they are equal to the two extremal values of the curvature radius. There are two important quantities which are invariant to the curvature tensor and these are the *mean curvature* and the *Gaussian curvature*. The mean curvature is the trace of the curvature tensor and is given by $H = c_1 + c_2$, it can be thought of as the average of the curvatures. The Gaussian curvature is the determinant of the curvature tensor and it is given by $K = c_1 c_2$.

To get an idea of the geometrical meaning of these quantities, we will look at the following. If $K = 0$, then the value of at least one the curvatures is zero and the local surface can be applied onto a flat plane. If $K > 0$, then the surface locally looks like a sphere and if $K < 0$, then the surface locally looks like a saddle. If $H = 0$ then the two principal curvatures are opposite to each other and the surface has saddle geometry and is locally extremal under small deformations of the surface.

The Gaussian curvature is named after the mathematician Gauss, who introduced it and studied its properties. One of the important properties of the Gaussian curvature is that the integral of it over the whole closed surface is a topological invariant. It is proportional to the number n_c of connected components and the number n_h of handles of the surface, and given by the Gauss-Bonnet theorem:

$$\oint dA K = 4\pi\chi_E = 4\pi\left(n_c - n_h\right)$$

This formula will be useful in a later section for the calculation of the curvature energy of the closed vesicle membrane.

A useful formula for the curvature is needed later on so we will start with the definition of the curvature of a curve:

$$c = \left| \frac{d\vec{T}}{ds} \right|$$

(2.4)

this states that the curvature is the derivative of the unit tangent vector with respect to the arc length of the curve, s. The unit tangent vector is given by:

$$\vec{T}(t) = \frac{\vec{r}'(t)}{|\vec{r}'(t)|}$$

(2.5)

where the prime indicates a derivative with respect to t, a generalized parameter. The curvature is easier to use if it is expressed in terms of the generalized parameter t, so one makes the following manipulations:

$$\frac{d\vec{T}}{dt} = \frac{d\vec{T}}{ds}\frac{ds}{dt} \qquad \text{and} \qquad c = \left| \frac{d\vec{T}}{ds} \right| = \left| \frac{d\vec{T}/dt}{ds/dt} \right|$$

(2.6 a, b)

where the equation 2.6a) is the chain rule. However, in equation 2.6b), the denominator ds/dt is simply equal to $|r'(t)|$ so the curvature is now expressed as:

$$c(t) = \frac{|\vec{T}'(t)|}{|\vec{r}'(t)|}$$

(2.7)

This form will be more useful.

A useful example is the curvature of a sphere of radius a. The two principal curvatures of this sphere will obviously be $1/a$. A diagram illustrating the two principle curvatures of saddle like surface is shown in figure 2.1.
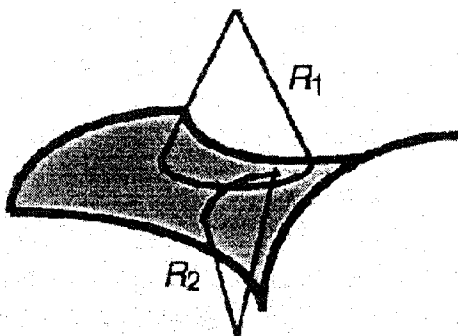
Fig2.1. Principle radii of curvature of a saddle-like surface. (Taken from Boal D, 2000)

2.3. Curvature-Composition Free Energy

2.3.1. Bending Energy

Displacing bilayer phospholipids from their equilibrium position requires energy input. A couple of ways to displace bilayer phospholipids is by compression, stretching or bending of the bilayer.

Membranes do not respond well to stretching. As the bilayer is stretched, it becomes thinner and its hydrophobic core (lipid tails) is increasingly exposed to water. The membrane will fail once it has been stretched to only about 2-5% of its equilibrium area. At this point a hole is formed that permits the phospholipid density to return to its optimal value and the membrane is effectively burst (Boal, 2002c). In light of this relatively low tolerance of the bilayer to stretch, we will only consider the bending contribution to the bulk conformational energy of the membrane.

The bending of a bilayer involves both the stretching of one layer of the compression of the other as shown in the figure 2.2.
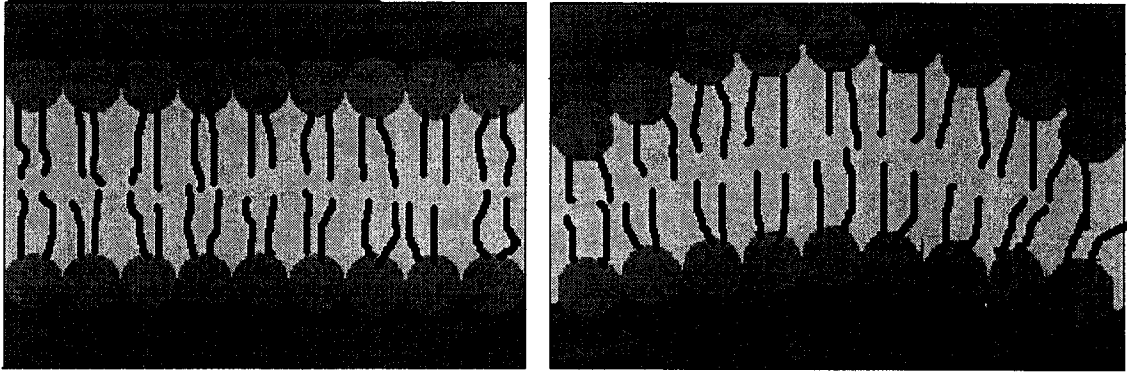
Fig 2.2 Bending a symmetric bilayer from a planer configuration (a) to a curved shaped (b) involves stretching (top) and compressing (bottom) the individual leaflets.

The bending energy per unit surface increases with the curvature. The simplest form of this energy contains contributions from the mean curvature $(C_1+C_2)^2$ and Gaussian curvature C_1C_2 where C_1 and C_2 are the principal curvatures described earlier. The bending energy density will then be as follows (Peliti, 1997b):

$$\Im = \frac{\kappa_b}{2}(C_1 + C_2)^2 + \kappa_G C_1 C_2 \qquad (2.8)$$

where the two parameters κ_b and κ_G are bending rigidity and the Gaussian rigidity, respectively. The parameters both have units of energy and are specific to the material of interest.

The total Gaussian bending energy of a given surface is given by the constant quantity $4\pi(n_c-n_h)$, where n_c is the number of connected components and n_h is the number of handles. The Gaussian bending energy is thus a topological invariant under continuous deformations of the vesicle. For example, if a spherical vesicle deforms into an ellipsoid, then the Gaussian bending energy does not change. Since we are concerned with shape changes with a constant topology, the Gaussian energy term can be neglected. Another modification will be to include the spontaneous curvature C_0, which reflects possible asymmetries in the two monolayers on the membrane. Asymmetries can occur in two

component systems (Safran, 1991) and will, therefore, depend on the local composition. C_0 will thus depend on the local composition of the membrane which will be discussed at a later section.

If the form of the energy density is selected so that the stable configuration occurs when the curvature is the same as the spontaneous curvature, the bending energy density for a given component becomes:

$$\Im = \frac{\kappa_b}{2}(C_1 + C_2 - C_0)^2$$

(2.9)

The bending rigidity κ_b is of the order 10^{-19} J, or few tens of $k_B T$ (Peliti, 1997c). Therefore, an isolated, unconstrained membrane undulates easily at room temperature. Many measurements of the bending rigidity have been done by analyzing the amplitude of the bilayer's thermal fluctuations for synthetic vesicles (Schneider *et al.*, 1984; Faucon *et al.*, 1989; Duwe *et al.*, 1990; Meleard *et al.*, 1997) or flat bilayer sheets (Mutz and Helfrich, 1990). Another approach examines the effective in-plane area of a membrane as produced by thermal fluctuations (Boal, 2002d).

A functional relationship between the bending rigidity and the thickness of the bilayer is predicted by a polymer brush model to give

$$\kappa_b \propto d_{bl}^2$$

(2.10)

where d_{bl} is the thickness of the bilayer (Boal, 2002d).

2.3.2. Coupling Energy of a Binary Mixture (Safran, 2003)

In two component systems there will be interactions between neighbouring molecules that contribute to the free energy of the system. We will examine thermodynamic and

structural properties on length scales much larger than molecular sizes. Therefore, we take into account excluded volume interactions between the hard cores of the molecules by putting the two components on a lattice whose sites are labeled by i = 1, ...N. We can use a lattice in which each site is the same area since we are studying a system of surfactants whose head groups are generally the same size but whose tail groups are different lengths. We denote component "A" by the variable $s_i = 1$ and denote component "B" by $s_i = 0$ where the index "i" indicates lattice site i. The interaction energy between two "A" molecules a distance $|\mathbf{R_i} - \mathbf{R_j}|$ apart is given by coupling energy J_{ij}^{AA} while the similar interaction between two "B" molecules is given by J_{ij}^{BB} and between an "A" and "B" pair is J_{ij}^{AB}. The microscopic Hamiltonian of this lattice-gas model is:

$$H = -\frac{1}{2}\sum_{ij} K_{ij}$$

(2.11)

where

$$K_{ij} = \left[J_{ij}^{AA}(1-s_i)(1-s_j)\right] + J_{ij}^{BB}s_i s_j + J_{ij}^{AB}\left[s_i(1-s_j) + s_j(1-s_i)\right]$$

(2.12)

The negative sign in the Hamiltonian indicates that the interactions are attractive while the "J" terms indicate the magnitude of the attractive interactions. The first term will be non-zero only when there are two "A" molecules at sites i and j, while the other terms follow similar considerations.

The Hamiltonian from equation 2.11 can be rearranged in such a way that redefines the zero of energy of the system. Ignoring this constant term, one can write the net interaction of the system as:

$$\frac{1}{2}\sum_{ij}\left[J_{ij}^{AA} + J_{ij}^{BB} - 2J_{ij}^{AB}\right]s_i\left(1 - s_j\right)$$ (2.13)

Therefore, if the number of attractive interactions between AA and BB pairs are more than those of the AB pairs, the system will tend to phase separate into an "A" rich phase and a "B" rich phase, maximizing the number of AA and BB pairs. The interaction Hamiltonian can thus be re-written in following simple form:

$$H = \frac{1}{2}\sum_{ij}J_{ij}s_i\left(1 - s_j\right)$$ (2.14)

where

$$J_{ij} = \left[J_{ij}^{AA} + J_{ij}^{BB} - 2J_{ij}^{AB}\right]$$ (2.15)

The partition function of this Hamiltonian is difficult to evaluate so we must introduce a variational method to find an approximate solution.

2.3.3. Variational Method

Consider a system described by an exact Hamiltonian, H. The probability distribution, P, of the system is given by the Boltzmann factor, $P \sim e^{-H/T}$; which is the result of the minimization of the total free energy parameterized by the probability distribution, P:

$$F^* = T\int d\Delta P\log P + \int d\Delta PH$$ (2.16)

where F^* is the exact free energy and Δ represents the phase space of the system. A variational approximation to the true Boltzmann weight and hence to the free energy can be obtained by considering a reference system, described by a Hamiltonian, H_0, which

contains several parameters and by minimizing F^* with respect to these parameters. Therefore, the free energy is approximated by:

$$F = T \int d\Delta P_0 \log P_0 + \int d\Delta P_0 H \qquad (2.17)$$

where $P_0 \sim exp(-H_0/T)$. In fact, it can be shown that the *exact* free energy, F^*, of the system with a Hamiltonian H obeys the inequality:

$$F^* < F = F_0 + \langle H - H_0 \rangle_0 \qquad (2.18)$$

where F_0 is the free energy of the model system and the average values are taken with respect to the Boltzmann factor $exp(-H_0/T)$ of the model Hamiltonian. Thus, if one chooses H_0 to have a given functional form with some unknown parameters, an approximation to the free energy may be derived by minimizing F as defined above with respect to these parameters so the lowest upper bound on F^*, is obtained. We can now use this variational method to help find an approximation to the exact free energy of the system.

2.3.4. Free energy of a Heterogeneous Binary Mixture

On the surface of the lipid membrane, the relative composition that is, the relative number fraction of "A" molecules, is given by ϕ and for "B" molecules is $1 - \phi$. The composition will not be homogenous throughout the system since the curvature will vary along the membrane surface and each component will have a different curvature preference than the other. It is thus necessary to use a model in which the composition changes along the surface – ie., $\phi(\mathbf{r})$ varies in space.

We will start with the lattice-gas model of a two-component system given in equation 2.14 and consider, for simplicity, only two-body interactions between the components. The Hamiltonian of the exact system, H, written as a function of the local composition variable at site i, s_i, where $s_i = 1$ represents an "A" molecule and $s_i = 0$ represents a "B" molecule. We then have:

$$ H = \frac{1}{2} \sum_{ij} J_{ij} s_i \left(1 - s_j\right) $$

(2.19)

where J_{ij} is the net interaction between the two components as before. In order to obtain phase separation of the mixture, the terms J_{ij} must be positive. However, as mentioned, the partition function for this Hamiltonian is difficult to evaluate because of the coupling between the sites. We will then invoke the variational method, as described in the last section, and construct a model Hamiltonian, H_0, a function of single-site variables only:

$$ H_0 = \sum_i T \beta_i s_i $$

(2.20)

where the factor of T is put in the definition of β_I for convenience. The parameters β_i are determined using equation 2.18 to derive the upper bound F, on the exact free energy, F^*, and then minimizing F with respect to the parameters β_i (with the constraint that the average composition is fixed) to determine the least upper bound and best estimate within the variational scheme. The integral depicted in the discussion of the variational scheme over all the degrees of freedom is of the form

$$ \int d\vec{p} \, d\vec{q} $$

(2.21)

but since we are using a discrete lattice model, we will use:

$$\prod_i \sum_{s_i=1,0} \qquad (2.22)$$

(ie., a product over all sites i of the sum over the two possible values of $s_i=0,1$).

The free energy of the model system, F_0, is given in terms of the partition function, Z_0, as follows:

$$F_0 = -T \log Z_0 \qquad (2.23)$$

$$(2.24)$$

$$Z_0 = \prod_i \sum_{s_i=1,0} e^{-\beta_i s_i} = \prod_i \frac{1}{1-\phi_i}$$

where $\phi_i = [1 + exp(\beta_i)]^{-1}$. One can show by taking the average with respect to $P_0 = exp[(F_0-H_0)/T]$ that $\phi_i = \langle s_i \rangle_0$; ϕ_i is the equilibrium average value of the local concentration variable, s_i in the ensemble described by H_0 and P_0. Since it is an average quantity ϕ_i can vary continuously from 0 to 1 and will be useful in constructing a continuous density profile for the system with an interface. A similar calculation gives

$$(2.25)$$

$$\langle H - H_0 \rangle_0 = \frac{1}{2} \sum_{ij} J_{ij} \phi_i (1 - \phi_j) - T \sum_i \beta_i \phi_i$$

Using the above equations we find that the upper bound on the exact free energy is

$$(2.26)$$

$$F = \sum_i [T\{(1 - \phi_i) \log(1 - \phi_i) + \phi_i \log \phi_i\}] + \frac{1}{2} \sum_{ij} J_{ij} \phi_i (1 - \phi_j)$$

The above free energy gives the energy of mixing for an inhomogenous system, that is, a system in which the local relative concentration ϕ_i varies in space. Such a system can possess a phase boundary between two regions in which one region is rich in "A" molecules and the other region is rich in "B" molecules.

The free energy from equation 2.26 also incorporates the edge tension energy of the interface between the "A" rich region and the "B" rich region, or in other words, between two phases. By examining the coupling term in the free energy, one can see that the coupling energy is relatively low in either of the phases (since ϕ is around 1 or 0 in either of these regions). But in the region of the interface, the local composition ϕ will be somewhere in between 1 and 0 which will raise the coupling energy, and therefore, account for the interfacial energy.

In the previous section, a discrete lattice-gas model was introduced to describe the interaction energy of the binary system. The length scales of two-component vesicles that are studied experimentally are often much larger than that of the individual molecules. For example, the head group of a membrane lipid has a bilayer surface area of around 40-70 Å^2 (Boal p140), whereas the membrane surface area is of the order 10^5 Å^2. This gives about 10^4 lipid headgroups across the membrane surface. It is therefore a valid approximation to take the discrete model to the continuum limit in order to describe two-component lipid bilayer vesicles.

To obtain the continuum limit, it is noted that

$$J_{ij}\phi_i\left(1-\phi_j\right) = \frac{1}{2}J_{ij}\left[\left(\phi_i - \phi_j\right)^2 - \phi_i^2 - \phi_j^2 + 2\phi_i\right]$$

(2.27)

In the continuum situation, we will have a free energy per unit volume instead of free energy per site in which the difference $\phi_i - \phi_j$ is converted to a gradient. For short-range, nearest-neighbour interactions, this gives

$$\left(\phi_i - \phi_j\right) \rightarrow a\nabla\phi$$

(2.28)

where a is the nearest-neighbour distance. The free energy of mixing can then be written as:

$$(2.29)$$

$$F = \int d\vec{r} \left[f_0 [\phi(\vec{r})] + \frac{1}{2} B |\nabla \phi(\vec{r})|^2 \right]$$

where $B = J/(2a)$, $J = \Sigma_j J_{ij}$ (like a local mean field), and with $\phi \rightarrow \phi(\mathbf{r})$ being the local value of the composition. The nonlinear, local part of the free energy per unit volume, f_0 is

$$(2.30)$$

$$f_0 = \frac{1}{a^3} \left(T[\phi \log \phi + (1-\phi) \log(1-\phi)] + \frac{J}{2} \phi(1-\phi) \right)$$

The above expression contains a gradient term, an entropy of mixing term and a term that is of the same form as the coupling term in the discrete lattice-gas model. We shall ignore non-local effects, which requires setting the gradient term to zero (Seifert, 1993), and the free energy of mixing will then be as follows:

$$(2.31)$$

$$F = \int d\vec{r} \left[\frac{1}{a^3} \left(T[\phi(\vec{r}) \log \phi(\vec{r}) + (1-\phi(\vec{r})) \log(1-\phi(\vec{r}))] + \frac{J}{2} \phi(\vec{r})(1-\phi(\vec{r})) \right) \right]$$

2.3.5. Simplification of the Entropy

From the determination of the two-component coupling energy there emerges an entropy of mixing term

$$\phi(\vec{r}) \log \phi(\vec{r}) + (1-\phi(\vec{r})) \log(1-\phi(\vec{r}))$$
$$(2.32)$$

which has the same form as Shannon's formula,

$$(2.33)$$

$$S = -K \sum_{j=1}^{M} P_j \ln P_j$$

where S is the entropy, K is a constant and P_j is the probability (or fraction) of component j. The entropy of mixing accounts for the disorder resulting from the mixing of the two components and varies along the surface of the membrane.

However, in real membrane systems, there are other contributions to the entropy. The first of these is the entropy due to the thermal undulations of the membrane, called the conformational entropy. If a membrane is confined not to be able to wander further than a certain distance from a plane, then a very large number of configurations that otherwise the membrane would have explored during the course of its thermally driven undulations will be forbidden to it, with a consequent loss of entropy (Jones, 2002c). This leads to an effective long ranged entropic potential that is important for a system of membranes. An additional source of entropy, called the translational entropy, arises as a result of the polydispersity of a system of aggregates, in which the vesicles have distribution of the sizes about a mean. Systems of polydispersed and relatively monodispersed unilamellar vesicles have both been observed in experiments (Neih, 2005).

In this project we follow Safran *et al.* (1991) and study equilibrium vesicles in the approximation where all the vesicles have (i) the same size and composition asymmetries (composition profile) and (ii) the same ratio of the two surfactants. By doing this, we will effectively ignore the conformational and translational entropy among other contributions and consider only the entropy of the mixing as derived for the continuous binary system.

2.3.6. Complete Free energy of the Vesicle

By including curvature and mixing effects, the total free energy of the vesicle is written as:

$$F_{vesicle} = F_{mixing} + F_{bending} \qquad (2.34)$$

$$F_{bending} = \oint dA \, \frac{1}{2}[\kappa_1 \phi + \kappa_2 (1 - \phi)][C_1 + C_2 - C_0]^2 \qquad (2.35)$$

$$F_{mixing} = \oint dA \left[\frac{J}{2}\phi(1 - \phi) + T[\phi \ln \phi + (1 - \phi)\ln(1 - \phi)] + u\phi \right] \qquad (2.36)$$

In the bending energy term, we have described the local bending rigidity in terms of the phenomenological parameters κ_1 and κ_2 where the first term denotes the bending rigidity contribution of component "A" and the second term for component "B". We see that κ_1 is coupled to the relative composition of component "A" and κ_2 is coupled to the relative composition of component "B". This mean-field like description of the local bending rigidity is somewhat simplified but is more manageable than a complete microscopic description that would include complicated interactions of the lipid tails, among other things.

At this point a more detailed description of the spontaneous curvature, C_0, can be given. We will use a model for C_0 where it will depend in a simple way on the local composition. By looking at the molecular geometry, we see that if the membrane locally consists of only long chain molecules ($\phi = 1$) or short chains ($\phi = 0$), then C_0 will be zero due to the symmetric bilayer. If the membrane locally has maximal mixing ($\phi=1/2$), then C_0 will be a maximum. This would occur because the membrane must curve in order to

obtain a closed packed configuration of the phospholipid molecules. A functional form

with respect to the local mixing ϕ that satisfies this is:

$$C_0(\phi) = C\phi(1 - \phi) \tag{2.37}$$

where C is a phenomenological parameter. This form is similar to that used by other

authors who have studied spontaneous curvature (Seifert and Lipowski, 1995).

The free energy of mixing consists of terms directly related to the composition

$\phi = \phi(\mathbf{r})$. To achieve the desired lipid composition, the Lagrange multiplier u is included.

This term is related to the chemical potential difference between the "A" and "B"

components.

2.3.7. Free Energy of The Bicelle

In order to describe the free energy of the bicelle we simply add an edge energy term

to the vesicle free energy:

$$F_{bicelle} = F_{bending} + F_{mixing} + F_{edge} \tag{2.38}$$

$$F_{edge} = \lambda \phi_{ave} \tag{2.39}$$

where

$$\lambda = 2\pi r \lambda' \tag{2.40}$$

The bending and mixing free energy density is integrated over the bilayer (which is

constrained to be flat) and the edge is treated separately. The bilayer curvature is

spatially isotropic (zero everywhere) so the composition profile, ϕ, will be homogenous

(thus denoted ϕ_{ave}) since the "A" and "B" components have different curvature

preferences. In this description, λ is the edge energy parameter, which is proportional to

the length of the bicelle edge perimeter $2\pi r$, where r is radius of the bicelle, and λ' is the effective edge energy per unit length as described in a previous section.

The edge energy is phenomenologically set to be proportional to the relative composition in the bilayer. This can be justified by the following. We note that the thickness of the bicelle increases as the relative composition ϕ increases, ie: the more long chain molecules there are in the bilayer, the thicker the bilayer will be. And, in turn, thicker bilayers will have a larger edge region, thus increasing the edge energy. The bicelle free energy as described by equation 2.38-40 can thus be used to represent the mixed bicelle phase (see figure 1.11) observed by Triba *et al* (2005).

2.4. Methods of Solution

2.4.1. Calculation of the Free Energy

We would like to solve for the free energy of the vesicle and the disk (equ 2.34-36 and 2.38-40). We start by dividing the free energy out by the bending rigidity, κ_1. We also use an appropriate unitless reference area since we will study constant area vesicles. This will give the following unitless expressions for the bending, mixing and edge energy:

$$\overline{F}_{bending} = \frac{F_{bending}}{\kappa_1} = \oint dA \frac{1}{2} [\phi + \overline{\kappa}(1 - \phi)][C_1 + C_2 - C_0]^2 \tag{2.41}$$

$$\overline{F}_{mixing} = \frac{F_{mixing}}{\kappa_1} = \oint dA \left[\frac{\overline{J}}{2} \phi(1 - \phi) + \overline{T}[\phi \ln \phi + (1 - \phi)\ln(1 - \phi)] + \overline{u}\phi \right] \tag{2.42}$$

$$\overline{F}_{edge} = \frac{F_{edge}}{\kappa_1} = \overline{\lambda}\phi_{ave} \tag{2.43}$$

where the barred terms, which are rescaled and unitless, can be considered phenomenological parameters.

It was mentioned earlier that κ_1 was the mean-field bending rigidity for component "A" and κ_2 for component "B". We would like to make qualitative comparisons of the theory with the experiments that have been discussed that typically use long chain DMPC molecules and short chain DHPC molecules. With this in mind, we designate component "A" with the long chain molecules and "B" with the short chains. From equation 2.10, $k = d^2$, the bending rigidity κ_1 will be larger than the bending rigidity κ_2 and the ratio κ_1/κ_2 (denoted by a barred κ in equation 2.41) will vary between zero and one. This ratio is thus a microscopic parameter that measures the relative molecular geometry of component "A" and "B". From equation 2.10 when "A" is much longer than "B", κ_1/κ_2 is small and when "A" approaches the same length of "B", κ_1/κ_2 increase up to unity.

In general there are many different kinds of stable shapes, that range from simple to relatively complicated, that are solutions to the free energy. These shapes generally need two variables to parameterize their surface. In order to simplify calculations we restrict the possible solutions to the class of *axisymmetric ellipsoids*. This kind of simplification where the shape is restricted has been done by other theoretical investigators (Safran, 1991; Chen, Higgs et al, 1997). This has the benefit that it can be parameterized by a single variable, the arc length (or equivalently the angular position) of the cross-sectional contour (see figure 2.3).
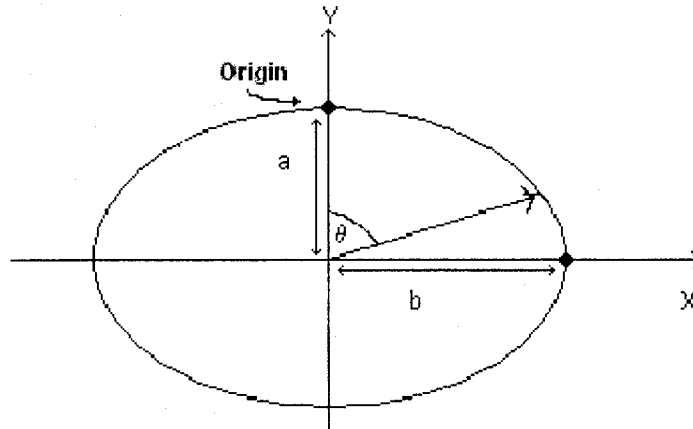
Figure 2.3. Digram of the a cross section of the axisymmetric ellipsoid where a is the length of the vertical axis and b is the length of the horizontal axis.

By using axisymmetric ellipsoids (Fig 2.3), the vesicle shape can be parameterized by the eccentricity, which is defined as the ratio of the axisymmetrical axis length to the horizontal axis.

The justification of this simplification is that in the aforementioned NMR and SANS experiments, the observed closed vesicle shapes consist of only spherical and oblate ellipsoidal shapes. Obviously, this theory also includes prolate ellipsoids.

The equilibrium vesicle states will be found by first using Lagrange's variational principle and minimizing the free energy with respect to the composition:

$$\frac{\partial F(\varepsilon, T, u, J, \kappa, \phi)}{\partial \phi} = 0$$

(2.44)

where ε is the eccentricity and T, u, J, κ are the rescaled, unitless parameters and are now denoted without bars. From this point on the rescaled parameters will continue to be denoted without bars. The self-consistent equation for the composition profile emerges from this which has the following implicit form:

$$\phi(\varepsilon, \theta) = g(\varepsilon, T, u, J, \kappa, \phi)$$

(2.45)

where g is a function of the eccentricity, the composition profile and the other parameters and θ is the angular position. It can be seen that the solution to this, which must be found numerically, will give the composition profile, $\phi(\theta)$, for different vesicle shapes of varying external conditions and material characteristics. These findings will be discussed in chapter 3. With the solution to the composition profile, the free energy can now be calculated.

2.4.2. Parameterization of the Membrane Surface

The shape transformations for axisymmetric, two-component membranes have been studied before (Julicher and Lipowsky, 1996; Hu, J-G and Ou-Yang, 1993). One common way to obtain shape equations consists of expressing the free energy in terms of the arc length S, and writing down the Euler-Lagrange equations using the appropriate constraints. Functional minimization gives a set of differential equations which have been used to calculate phase diagram for axisymmetric vesicles in spherical and toroidal topologies (Seifert, U., 1991; Seifert, U. et al., 1991; Berndl et al., J., 1990). One can also do the above by using the distance between the axis of symmetry and the contour as the parameter, instead of the arc length (Hu, J-G., Ou-Yang, Z-C, 1993).

In this project we parameterize with the angular position of the arc length and express the curvature and area in terms of this. These are then substituted in the free energy functional and this is integrated over with respect to the arc length. The detailed calculations are given in the appendix.

2.4.3 Calculation of the Phase Diagram

Stable vesicle shapes are found by examining the energetics of the system with respect to the eccentricity. It is possible to have three different vesicle shapes from the vesicle model: axisymmetric oblates, prolates and spheres. From the energetics of the system, the temperature vs. chemical potential phase diagrams are determined. These are used to construct temperature vs. average composition diagram, which are more appropriate for comparison with experimental data. This is relevant for comparing our theoretical model with the SANS results. This will be the subject of chapter 3.

In chapter 4 the bicelle phase will be examined. We simply compare the energies of the bicelle and vesicle and construct the phase diagram for vesicle and bicelle morphologies which will be compared to the NMR and SANS results.

Appendix A to Chapter 2

Parameterization of the Membrane Surface

The shape of the axisymmetric vesicle is defined by the shape of the cross section of the vesicle given by figure 2.4. We use as the independent parameter the angle θ. The arc length is parameterized as follows:

$$S = S(\theta) \qquad (2.A.1)$$

and so is x-coordinate and y-coordinate:

$$x = x(\theta) \quad y = y(\theta) \qquad (2.A.2a, b)$$

The area of the vesicle is then as follows:

$$(2.A.3a,b)$$

$$A = \oint dA = 2\pi \int_0^{2\pi} x S' d\theta, \quad S' = \frac{dS}{d\theta}$$

The derivative of S with respect to the angle in terms of the x and y-coordinate will also be needed:

$$S' = \frac{dS}{d\theta} = \sqrt{\left(\frac{dx}{d\theta}\right)^2 + \left(\frac{dy}{d\theta}\right)^2}$$

(2.A.4)

The curvature was given in equation 2.7 as follows:

(2.A.5)

$$c(t) = \frac{|\vec{T}'(t)|}{|\vec{r}'(t)|}$$

where the numerator contains the derivative of the tangent vector and the denominator contains the derivative of the position vector. There are two principle curvatures and in order to establish these, we must set up a coordinate system for the two dimensional membrane surface. The first component, the angle of the cross-sectional arc length, has already been given. The other component, given in figure 2.4, is the radial position given by the angle, ϕ. The tangent with respect to θ is given in the diagram by the angle ψ:

$$\psi = \psi(\theta)$$

(2.A.6)

$$\psi' = \frac{d\psi}{d\theta}$$

(2.A.7)

and the position is the arc length, S. This gives for the first principle curvature:

(2.A.8)

$$c_1 = \frac{\psi'}{S'}$$

The second principle curvature is given by

(2.A.9)

$$c_2 = \frac{\sin\psi}{x}$$

We would like to write out the local curvature in terms of the eccentricity and the angular position. The x and y-components are given as follows:

$$x = a \sin \theta \qquad\qquad (2.A.10)$$

$$y = b \sin \theta \qquad\qquad (2.A.11)$$

where a and b are the length of horizontal and vertical axis, respectively, and are shown

in the following diagram:
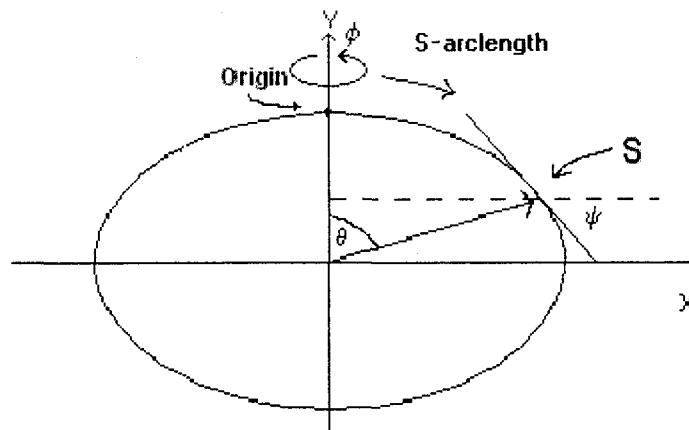
Figure 2.4. Cross section of an axisymmetric ellipsoid. The arc length from the origin is given by S which parameterizes the surface.

In order to express ψ as function of θ we consider the following relation for the tangent

angle:

$$\tan \psi = -\frac{dy}{dx} \qquad\qquad (2.A.12)$$

and the relation between the x and y component:

$$\frac{x^2}{a^2} + \frac{y^2}{b^2} = 1 \rightarrow y = b\sqrt{1 - \frac{x^2}{a^2}} \qquad\qquad (2.A.13)$$

Now we take the derivative of y from (2.A.13) with respect to x:

$$\frac{dy}{dx} = -\frac{b^2}{a^2}\frac{x}{y} = -\frac{b}{a}\tan \theta \qquad\qquad (2.A.14)$$

where the relation $x/y = (a/b)\tan\theta$ has been used.

At this point, we will simplify the calculations by using the eccentricity parameter:

$$\varepsilon = \frac{b}{a} \qquad (2.A.15)$$

as described in section 2.4.1 and equation 2.A.14 becomes

$$\frac{dy}{dx} = -\varepsilon^2 \frac{x}{y} = -\varepsilon \tan \theta \qquad (2.A.16)$$

We can now express ψ in terms of θ by relating the expression from (2.A.16) for dy/dx:

$$\tan \psi = \varepsilon \tan \theta \rightarrow \psi = \tan^{-1}\left[\varepsilon \tan \theta\right] \qquad (2.A.17)$$

We can now take the derivative of ψ with respect to θ is needed for the first principle curvature:

$$\psi' = \frac{d\psi}{d\theta} = \frac{1}{1+\varepsilon^2 \tan^2 \theta} \frac{\varepsilon}{\cos^2 \theta} = \frac{\varepsilon}{\cos^2 \theta + \varepsilon^2 \sin^2 \theta} \qquad (2.A.18)$$

The arc length, S, must also be expressed in terms of θ. We start out with the definition of the arc length:

$$S = \int_0^\theta d\theta' \frac{dS}{d\theta'} = \int_0^\theta d\theta' \sqrt{\left(\frac{dx}{d\theta'}\right)^2 + \left(\frac{dy}{d\theta'}\right)^2}$$
$$= \int_0^\theta d\theta' \sqrt{a^2 \cos^2 \theta + b^2 \sin^2 \theta} \qquad (2.A.19)$$

Using the Leibniz rule for differentiation of integrals:

$$S' = \frac{dS}{d\theta} = a\sqrt{\cos^2 \theta + \varepsilon^2 \sin^2 \theta} \qquad (2.A.20)$$

The first principle curvature can now be obtained:

$$(2.A.21)$$

$$c_1 = \frac{\psi'}{S'} = \frac{\varepsilon}{a\left(\cos^2\theta + \varepsilon^2 \sin^2\theta\right)^{\frac{3}{2}}}$$

The second principle curvature is relatively easier to find. It is as follows:

$$(2.A.22)$$

$$c_2 = \frac{\sin\psi}{x} = \frac{\sin\left[\tan^{-1}(\varepsilon\tan\theta)\right]}{a\sin\theta}$$

where the appropriate equation for $\psi(\theta)$ and $x(\theta)$ has been used.

From these expressions, we see that c_1 and c_2 vary with θ, ie: along the surface of the vesicle.

Appendix B to Chapter 2

Vesicle Free Energy In Terms of θ and ε

In chapter two, the free energy of the vesicle was given by equation 2.41-43. We will now write these in terms of θ and ε. We will simplify the curvature energy by introducing a curvature term, K, as follows:

$$(2.B.1)$$

$$\frac{1}{a^2}K(\theta,\varepsilon) = \left[\frac{\phi}{2} + \frac{\kappa}{2}(1-\phi)\right](c_1 + c_2 - c_0)^2$$

where

$$K(\theta,\varepsilon) = \left[\frac{\phi}{2} + \frac{\kappa}{2}(1-\phi)\right]\left\{\varepsilon\frac{1}{\left(\cos^2\theta + \varepsilon^2\sin^2\theta\right)^{3/2}} + \frac{\sin\left[\tan^{-1}(\varepsilon\tan\theta)\right]}{\sin\theta}\right\}^2 \quad (2.B.2)$$

The free energy functional must be integrated over the whole membrane surface which can be done by using the following:

$$\oint dA = 2\pi \int_0^\pi x S' d\theta$$

$$= 2\pi a^2 \int_0^\pi d\theta \sin\theta \sqrt{\cos^2\theta + \varepsilon^2 \sin^2\theta}$$

where S' has now been written as:

$$S' = a\sqrt{\cos^2\theta + \varepsilon^2 \sin^2\theta} \qquad (2.B.4)$$

and x is given from equation 2.A.10. The free energy of bending and mixing, which are

written in unitless form, are now giving as follows:

$$(2.B.5)$$

$$F_{bend} = 2\pi \int_0^\pi d\theta \sin\theta \sqrt{\cos^2\theta + \varepsilon^2 \sin^2} K(\theta, \varepsilon)$$

$$(2.B.6)$$

$$F_{mixing} = 2\pi \int_0^\pi d\theta \sin\theta \sqrt{\cos^2\theta + \varepsilon^2 \sin^2\theta} \{a^2 J\phi(1-\phi)$$

$$+ a^2 T[\phi \ln\phi + (1-\phi)\ln(1-\phi)] + a^2 u\phi\}$$

Minimizing the free energy functional with respect to the composition profile gives the

self-consistent equation for the composition profile, as mentioned in 2.4.1. This gives:

$$(2.B.7)$$

$$\phi = \frac{1}{2}\left[1 - \tanh\left\{\frac{\left[\frac{1}{a^2}K(\theta,\varepsilon) + u - 2J\phi\right]}{2T}\right\}\right]$$

3. RESULTS FOR VESICLES

3.1. Intoduction

The main results of this section come from the calculation of the composition profile and the phase diagram in the temperature vs. total composition regime (T vs ϕ_{av}). The composition profile is simple to find and is described in 2.4.1. The T vs ϕ_{av} phase diagram is not as straightforward to find and requires the calculation of the temperature vs. chemical potential phase diagram (T vs. u). The results have been obtained using numerical methods with FORTRAN 90.

3.2. Results

In this section we will calculate the T vs. u diagram for specific values of the bending rigidity, κ, the coupling, J, and the spontaneous curvature, c_0, for constant area vesicles. The variable, u, is actually related to the chemical potential difference of the two components but we will nevertheless refer to it as the chemical potential.

The coupling parameter, J, is kept at 0.5 and we do not show graphs with variations in J since we are interested in bending effects, which are more directly related to the curvature parameters κ and c_0.

The free energy vs. eccentricity (F vs. ε) graph is plotted for a given range of temperature and chemical potential. For each point (u, T) on the phase diagram, the stable and meta-stable shapes (denoted by ε) are found from the F vs. ε graph. The phase diagrams for different values of κ are as follows:
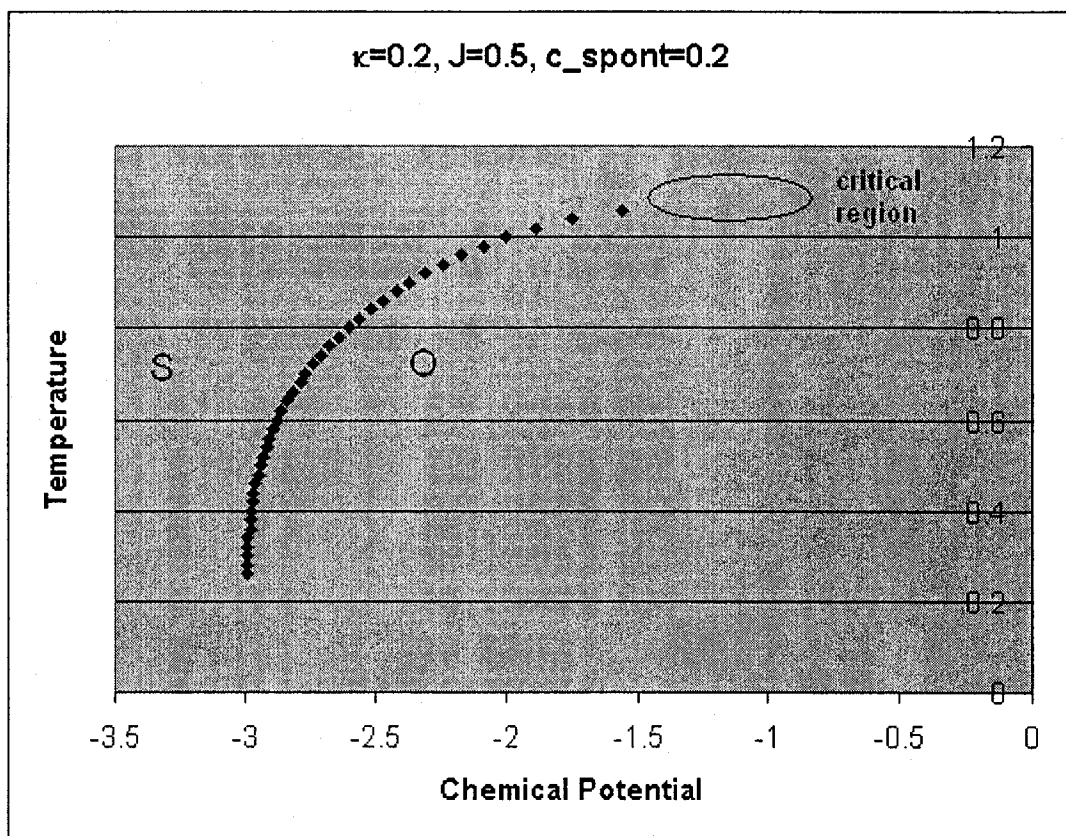
Figure 3.1.

Figures 3.1-6. Temperature vs chemical potential phase diagram. S represents the region corresponding to a spherical vesicle, O represents the region corresponding to oblate ellipsoid vesicles. The transition between these two regions are separated by the phase boundary. Toward the critical point (oval), the transition gradually disappears.

k=0.3, J=0.5, c_spont=0.2
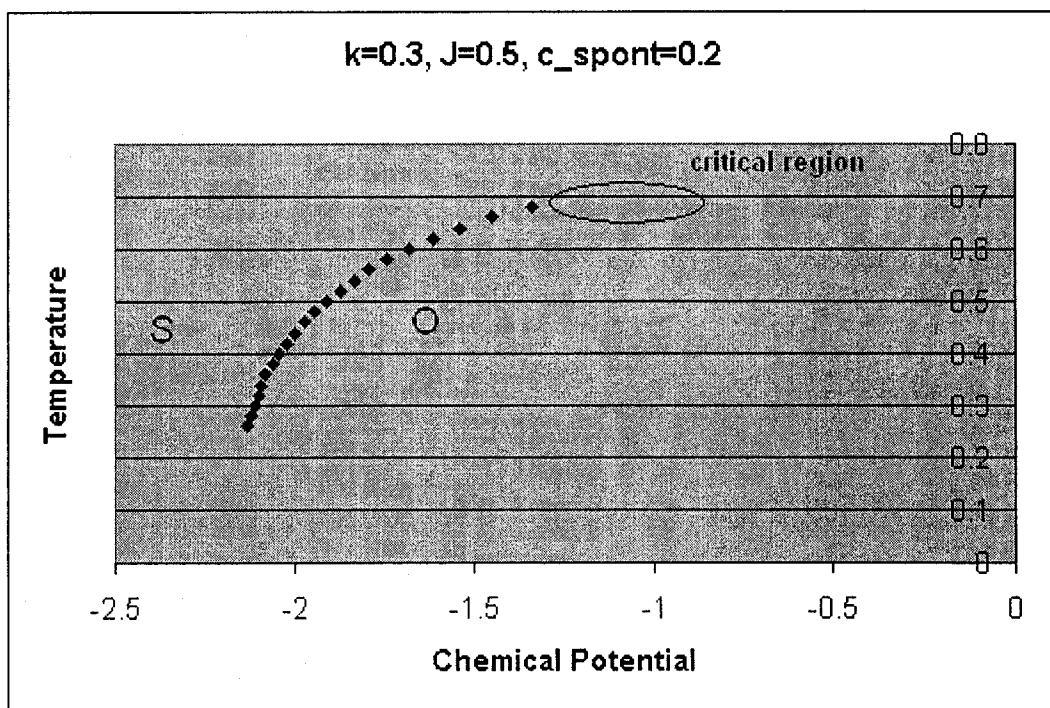
Figure 3.2. Caption below fig. 3.1.

κ=0.35, J=0.5, c_spont=0.2
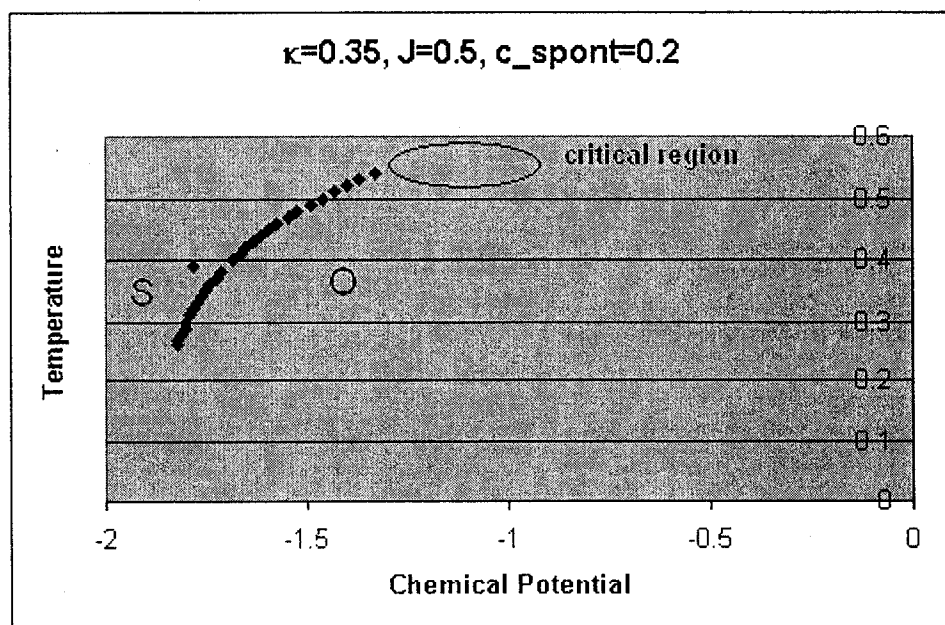
Figure 3.3. Caption below fig. 3.1

In figures 3.1-3, the data points map out the phase boundary for a discontinuous

transition in the temperature vs. chemical potential plane. This transition is from the

spherical state ($\varepsilon \sim 1$) denoted by the letter "S" to the oblate state ($\varepsilon \sim 0.5$) denoted by the

letter "O". Prolate shaped vesicles ($\varepsilon > 1$) are not observed for vesicles of constant area. A general phenomena that is not illustrated in the graphs is a weak, almost continuous change from the oblate state back to the sphere state with further increase of the chemical potential. This occurs around $u = -0.6$ to $u = -0.8$. The phase boundary line disappears at high temperature and chemical potential. At this region (the critical point), the transition disappears and for temperatures higher than this region, the spherical state is favoured for the whole range of chemical potential. In the region about the critical point, the free energy minima become very shallow and this gives rise to higher thermal fluctuations in the eccentricity.

The shape of the phase boundary is generally the same for all values of the relative bending rigidity, coupling parameter and spontaneous curvature but as the parameters are varied, the phase boundary changes in size and location as we will now discuss.

In the graphs shown thus far, J and c_0 are held constant while the κ is varied from 0.2 and increased. It is seen that for low κ, the critical point occurs at high temperature ($T \sim$ 1.1) and as κ is increased, the critical point is lowered in temperature. For even lower κ ($\kappa = 0.1$) the critical point is as high as $T = 2.1$ (graph not shown). If κ is increased further than 0.35, then the critical point will not be much higher than the initial temperature and the phase diagram consists almost completely of spherical vesicles (graphs are not shown for this).

The phase diagrams for different values of the spontaneous curvature, c_0, are now shown:
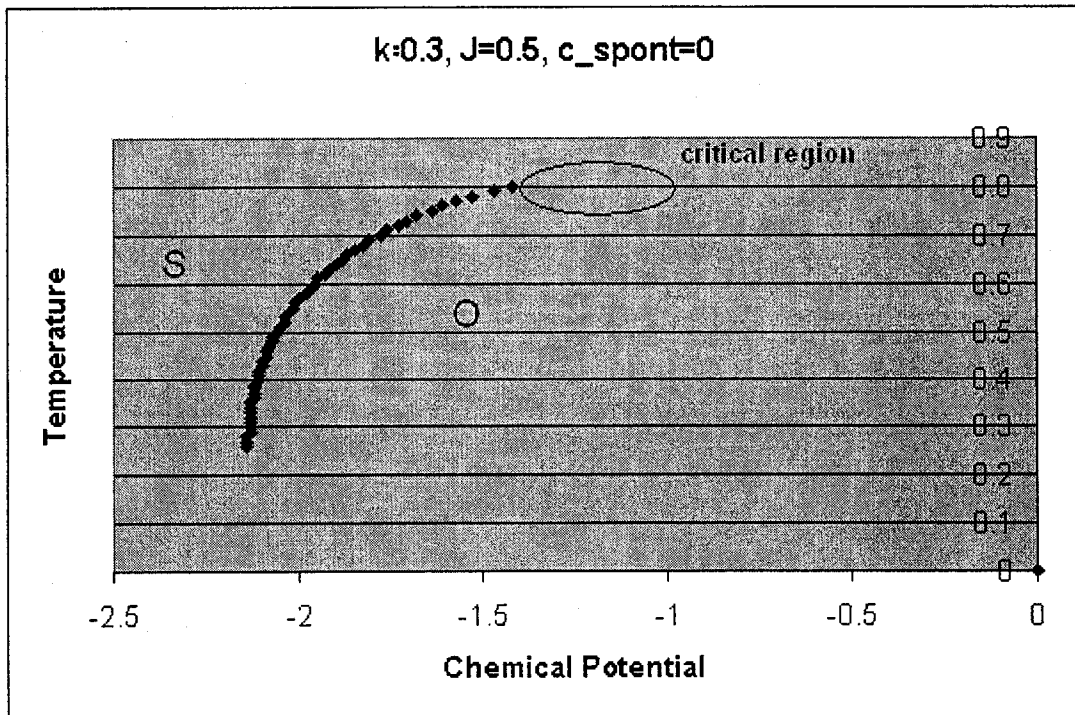
Figure 3.4. Caption below fig. 3.1.
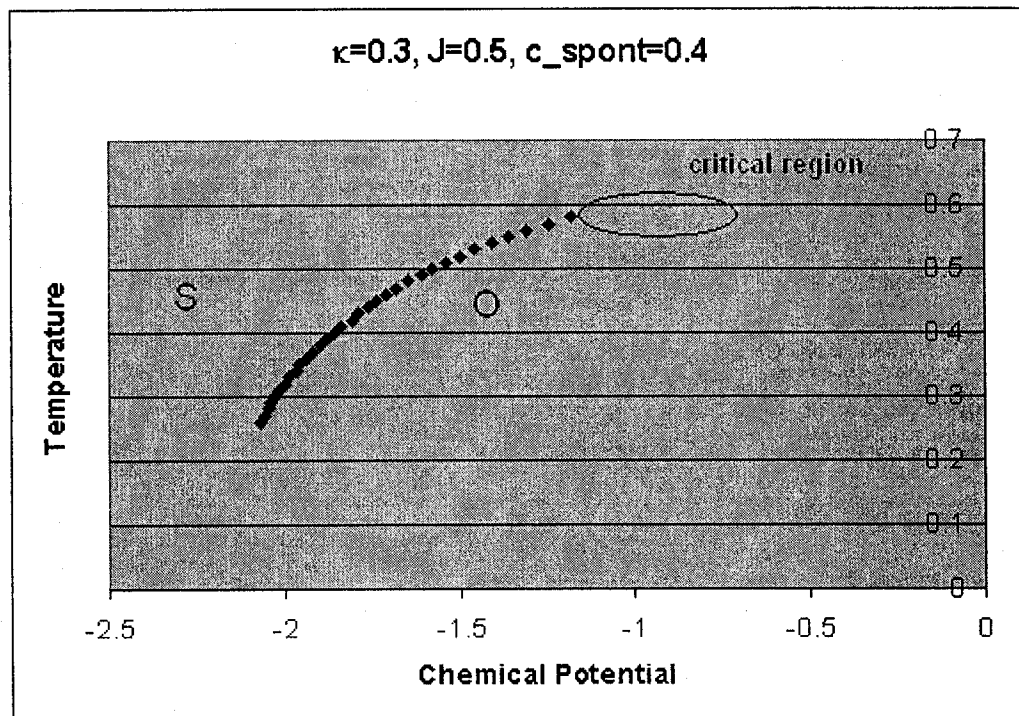
Figure 3.5. Caption below fig. 3.1.
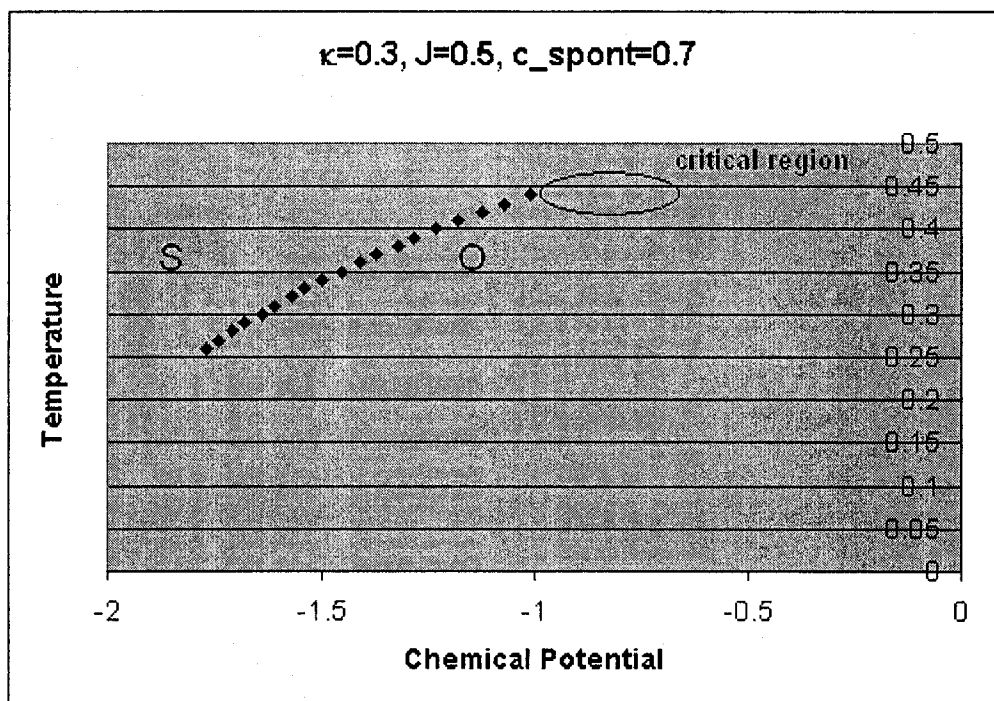
Figure 3.6. Caption below fig. 3.1.

In these diagrams, we see a similar effect on the phase boundary upon increasing the spontaneous curvature (denoted c_spont in the figures) as with increasing κ. The critical point for zero spontaneous curvature occurs at the highest temperature ($T = 0.8$) and the critical temperature is lowest for $c_0 = 0.7$ at $T = 0.45$.

We now show the T vs. ϕ_{av} phase diagrams, which are obtained by calculating the average composition (eq. 3.1) of the equilibrium phase at fixed temperature (T) and chemical potential (u). The coexistence boundaries are found by determining, at a fixed temperature, the chemical potential at which the sphere and oblate phases are equally stable. The coexistence boundary then corresponds to the average compositions of the sphere and oblate at this point (T, u) for the two stable eccentricities at the phase boundary in the T vs. u phase diagrams.

$$(3.1)$$

$$\phi_{ave} = \frac{\oint dA\,\phi(\vec{r})}{\oint dA}$$


κ=0.2, J=0.5, c_spont=0.2
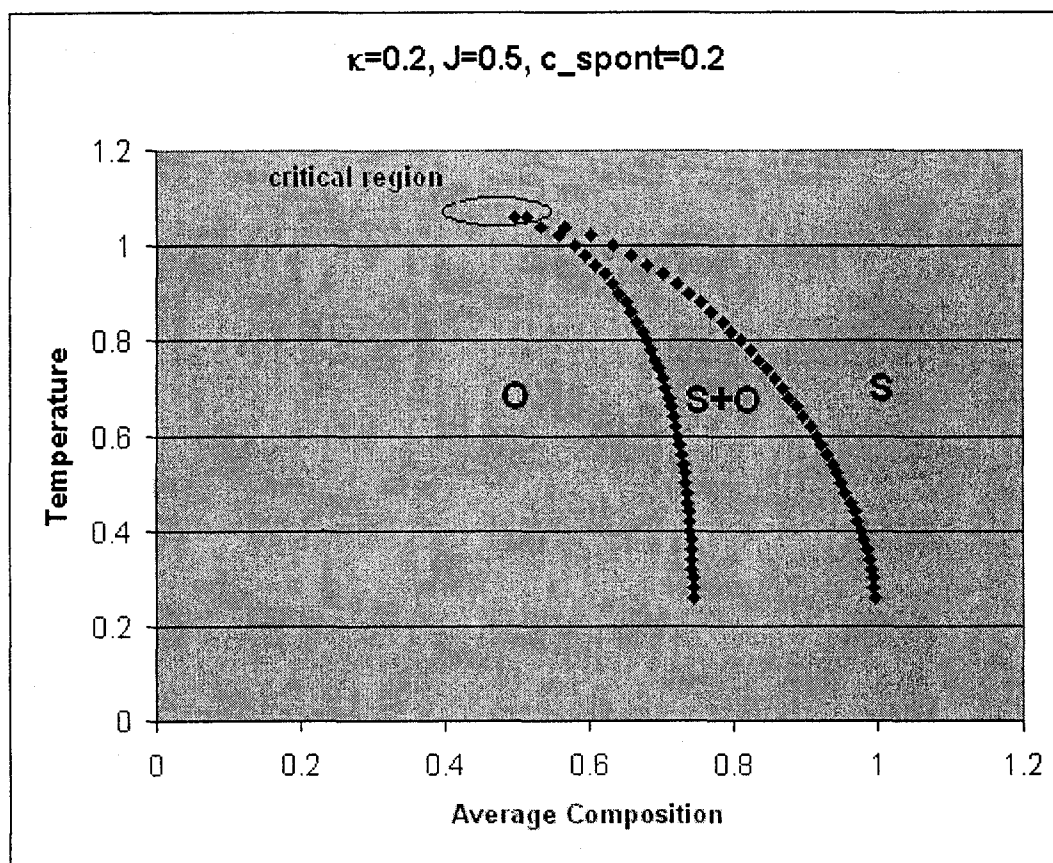
Figure 3.7.

Figures 3.7-10. Temperature vs average composition phase diagram. S represents spherical vesicles, O represents oblate shaped vesicles. S+O is the coexistence region. In this region, spheres and oblates both exist, however the average composition of O will be that at the left boundary and of S will be that at the right boundary. The critical region is denoted by the oval.
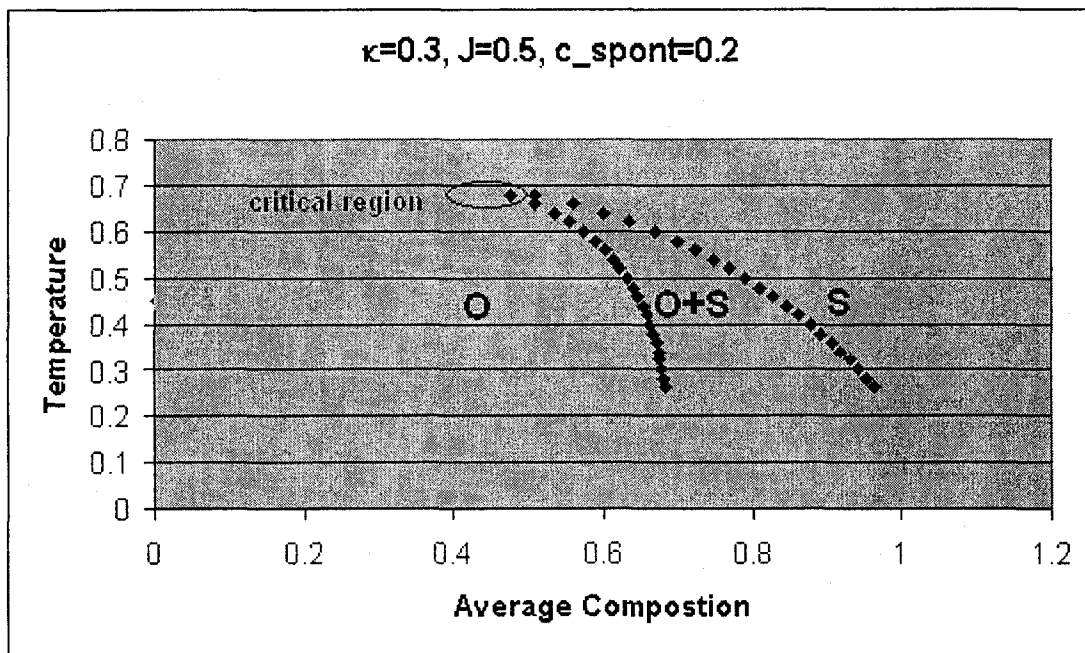
Figure 3.8. Caption below fig 3.7.
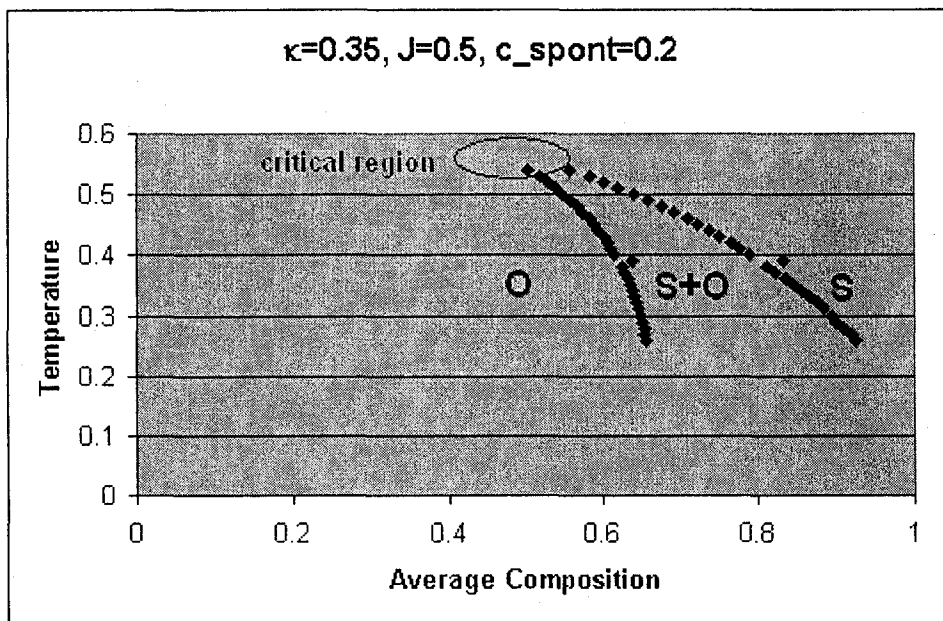
Figure 3.9. Caption below fig 3.7.

κ=0.3, J=0.5, c_spont=0
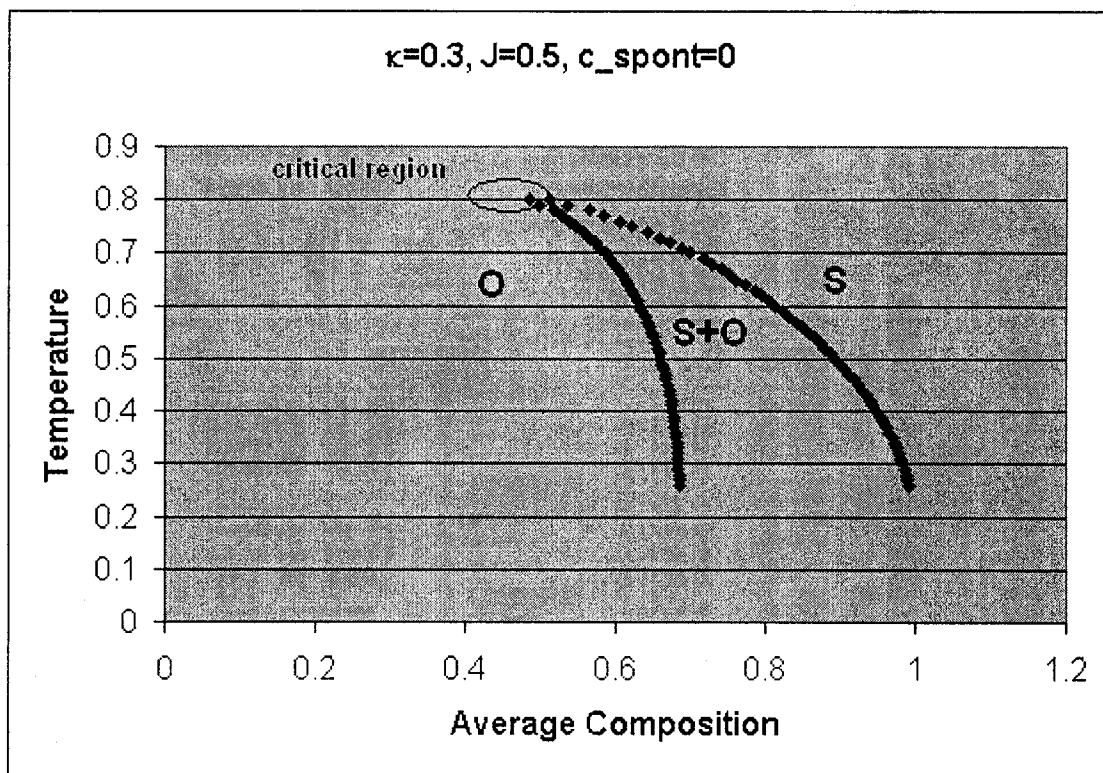
Figure 3.10. Caption below fig 3.7.

In the above figures S denotes the region where the spherical vesicle is stable, O denotes

where the oblate vesicle is stable and the region where the two states co-exist is given by

$S+O$. Regions of high average composition, ϕ_{ave}, correspond to low chemical potential

and low ϕ_{ave} to high chemical potential. The coexistence regions coincide with the phase

boundary in the T vs u phase diagram and the tip at the top of the coexistence region is

the critical point. Above this point, only the spherical state exists and there is no phase

transition.

As the bending rigidity, κ, is increased we see that the critical point is lowered in

temperature and the coexistence region shifts slightly to smaller values of ϕ_{ave}. For $\kappa =$

0.2 the edge of the coexistence region is at the end of the ϕ_{ave} axis and as κ is raised to

0.35, it shifts to about $\phi_{ave} = 0.93$. In general, the oblate region of the phase diagram

decreases with increasing κ. It is hard to investigate higher values of κ, however, because the spherical phase begins to dominate the phase diagram, as mention earlier.

Increasing the spontaneous curvature, c_0, has the same effect as raising κ. For $c_0 = 0$ in figure 3.10, we see that the edge of the coexistence region is at the end of the ϕ_{ave} axis and when c_0 is raised to 0.7 (not shown), the edge shifts to $\phi_{ave} = 0.8$, decreasing the oblate region of the phase diagram.

The composition profiles for various stable vesicles are also given:
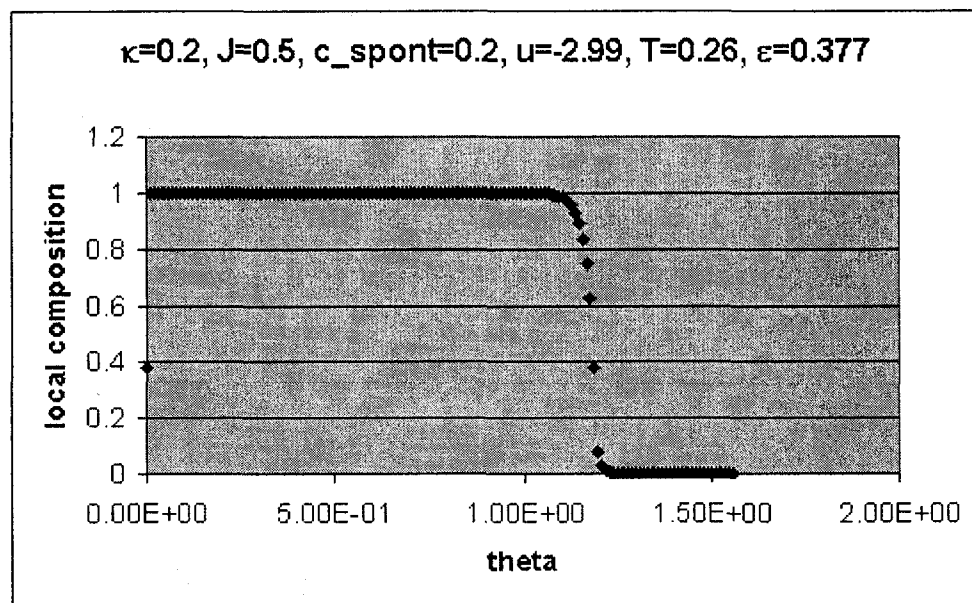
Figure 3.11.

*Figures 3.11-14. Composition profiles for different vesicles. The interpretation of this is given in figure 3.16.*

κ=0.2, J=0.5, c_spont=0.2, u=-2.99, T=0.26, ε=0.989
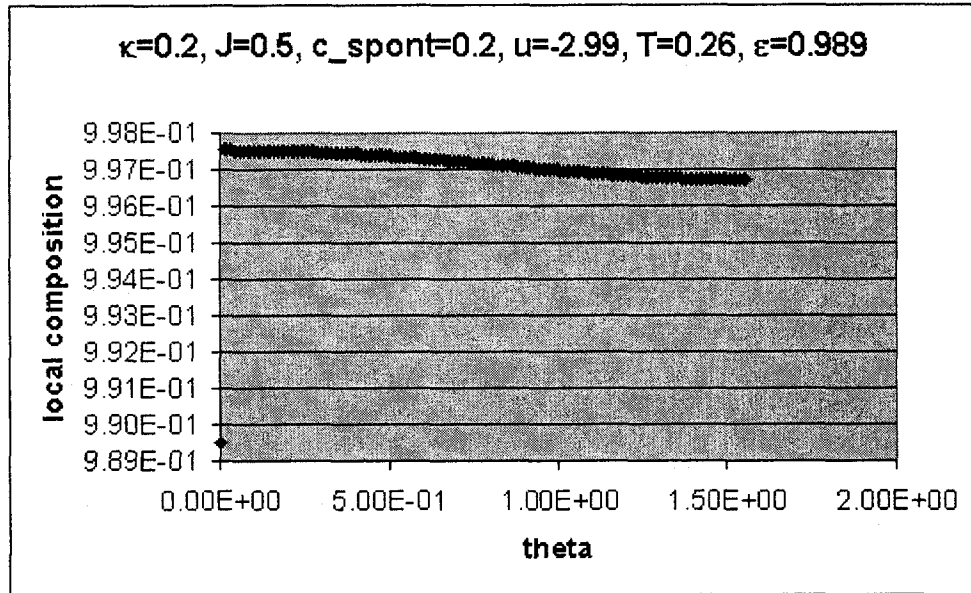
Figure 3.12. Caption below fig. 3.11.

κ=0.2, J=0.5, c_spont=0.2, u=-2.00, T=1.00, ε=0.438
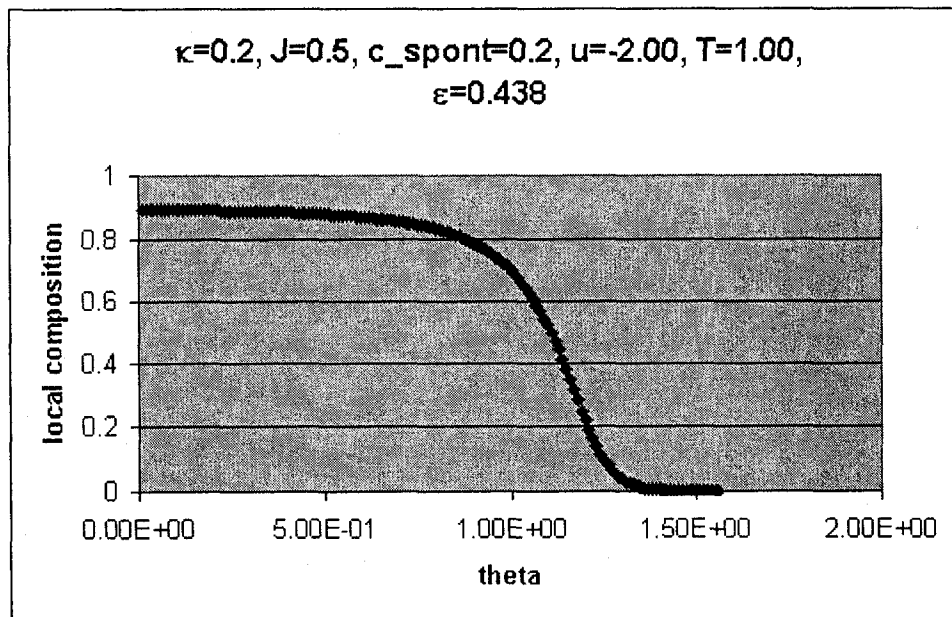
Figure 3.13. Caption below fig. 3.11.

κ=0.2, J=0.5, c_spont=0.2, u=-2.00, T=1.00, ε=0.975
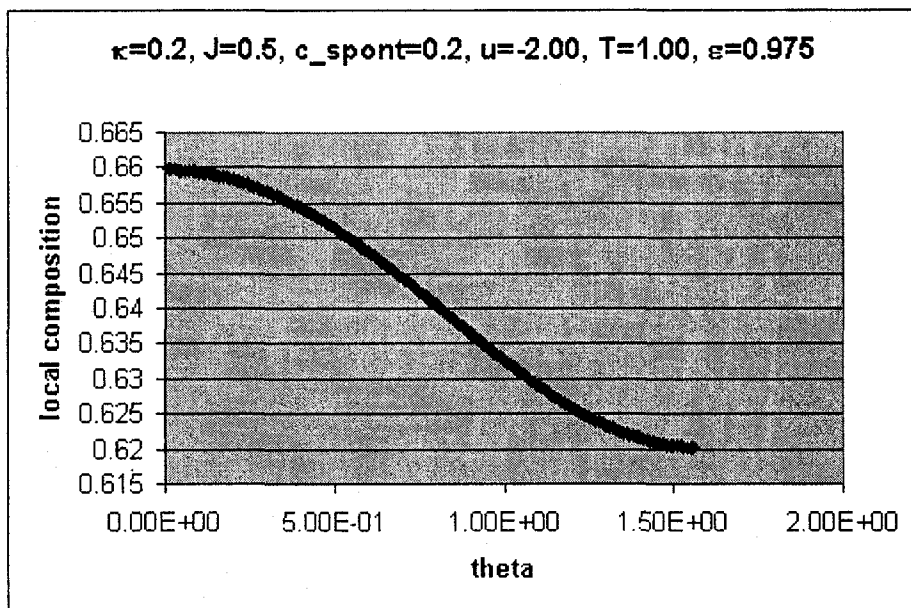
Figure 3.14. Caption below fig. 3.11.

k=0.2, J=0.5, c_spont=0.2, u=-2.0, T= 2.0, e=0.98
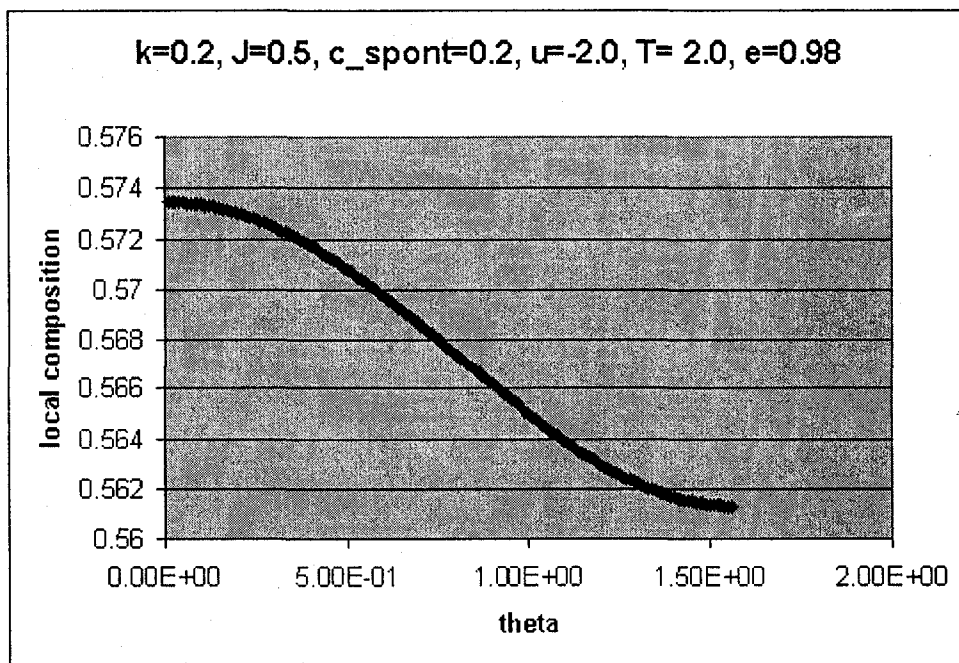
Figure 3.15. Composition profile for a high temperature sphere.

Since the vesicles are axisymmetric, we plot only up to $\pi/2 = 1.571$ which covers half of

the cross-sectional contour. The other half of the contour will simply be the mirror image

of the first half. The interpretation of these plots is shown in the next figure:
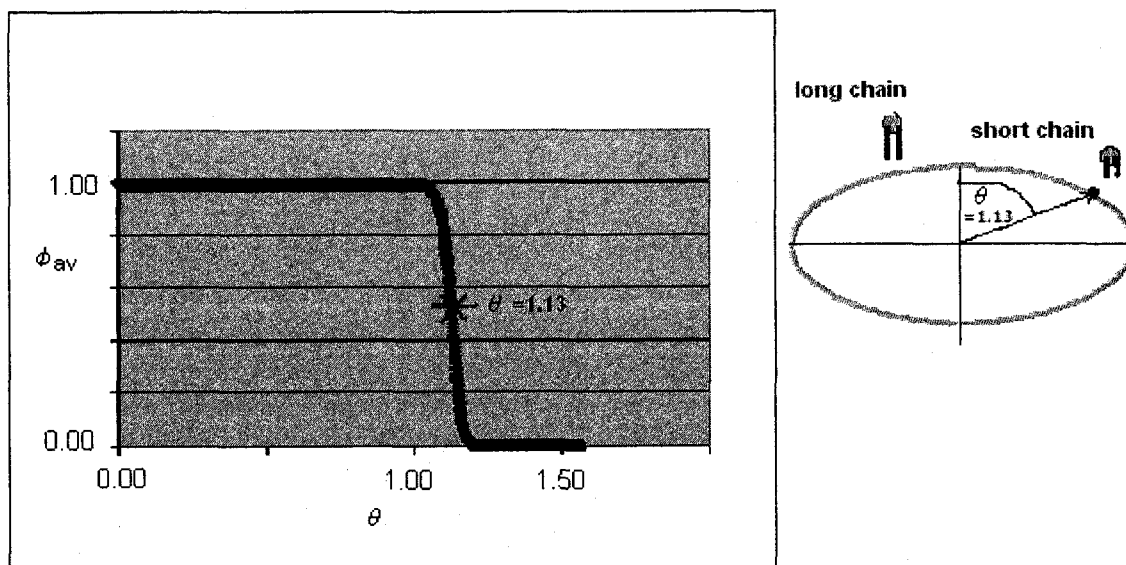
*Figure 3.16. A sample graph of the composition profile. The angle theta of the horizontal axis of the graph denotes the position on the cross sectional contour on the right diagram. The graphs go up to π/2, which is the first quadrant of the diagram on the right.*

The first two figures are the composition profile for the oblate state ($\varepsilon = 0.377$) and the spherical state ($\varepsilon = 0.989$) which occur at either side of the phase boundary of figure 3.1 for lower temperature ($T = 0.26$, $u = -2.99$). With the oblate state, we see domain segregations where the composition varies abruptly from very high at almost one to very low. This is a general feature of oblate shapes. The long chain molecules are located at the relatively flat top and bottom regions and the short chains are along the higher curvature sides of the vesicle. In contrast, for the spherical vesicle no domain segregation occurs and the composition remains relatively constant.

The second set of figures are for the oblate and spherical state at the phase boundary for higher temperature ($T = 1.00$, $u = -2.00$). The oblate composition profile in this case is less sharp than that of the lower temperature oblate. The phase boundary between the two components is somewhat blurred. In addition to this, there is less segregation between the two components in the domains compared to the low temperature oblates.

The high temperature spherical vesicle has a less homogenous composition profile than for low temperatures.

3.3   Discussion

As already apparent in the results section, the shape changes of the vesicles can be described by a phase diagram in the T vs u plane or the T vs ϕ_{av} plane while the locations of the phase boundaries can vary upon changing the phenomenological parameters κ and c_0. In this section we will relate our theoretical results to some experimental works that have been done and discuss the thermodynamic behavior of these structures.

In all of our results, the spherical vesicle is stable for high temperatures and the oblate for lower temperatures with the highest temperature for stable oblates just below the critical point. We see in the composition profile of the high temperature sphere (figure 3.15) a much higher degree of mixing than the lower temperature oblates which is expected since the entropy of mixing increases at higher temperatures.

In figures 3.1-3 and 3.7-9, we show the results of increasing the bending rigidity and observe that the critical point is lowered as κ increases, destabilizing oblate vesicles in favour of spherical vesicles. This can be understood in terms of the relative bending rigidities of the two components and how this is related to the curvature variations along the vesicles. As mentioned in Chapter 2.3.1, κ describes the relative molecular geometry of the two components and, by equation 2.10, approaches unity as the two components get closer in length. If both molecules have similar geometries (higher κ), the local bending rigidity and hence the curvature cannot vary too much. This would favour the formation of a spherical vesicle. However, if both molecules have greater differences in

molecular geometry (lower κ) the range of the local bending rigidity and hence curvature is greater. Vesicles can then form oblate shapes, which have wider curvature variations, with less of an energy penalty. This is what we see in figures 3.1-3 and 3.7-9 where oblates are more stable for lower κ.

In figure 3.4-6, 3.7, and 3.10 we see that the effect of increasing the spontaneous curvature, c_0, is the same as increasing κ in that it increases the stability of spherical vesicles. c_0 is a measure of curvature preference so as it is increased we expect vesicles that posses a particular curvature, namely spheres.

In figures 3.11-14, we see directly how the local curvature is co-related to how the long chain and short chain molecules are situated. The low curvature top and bottom region of the oblate are high in long chain molecules, which have higher bending rigidity, while the high curvature side of the vesicle is high in short chains of low bending rigidity, which is expected. The composition profile for the low temperature oblate and sphere phase exhibits a high degree of segregation as well, resulting in relatively low entropy. This type of behavior where the short chain molecules occupy high curvature regions and the long chains occupy lower curvature regions is generally seen in these systems (Baumgart, T., Hess, S. T., Webb, W. W. 2003).

Figures 3.11-14 also exhibit the result of varying the temperature. At higher temperature the oblate and sphere both exhibit a smaller degree of segregation raising the entropy of mixing which is also expected. This high temperature mixing is reminiscent of the inter-domain mixing reported by Triba et al. (2005) for two-component bicelles, which have been mentioned in section 1.6.

An important result is the presence of a sharp boundary between a long chain rich region and short chain rich region on the oblates. This high segregation is reminiscent of domain boundaries that have been observed in various experiments (Veatch, S. L. and Keller S. L. 2005; Baumgart, T., Hess, S. T., Webb, W. W. 2003).

The constant curvature of the spherical vesicle can be understood in terms of its generally homogenous composition profile (figures 3.13 and 3.14). The local bending rigidity is dependent upon the local mixing. But in spheres we see that the local mixing and hence the local bending rigidity does not vary too much. As mention earlier, the constant bending rigidity tends to forms constant curvature, *ie:* spherical, structures. This effect is different than the previous effect where increasing κ stabilizes spheres in that for the present effect it is the *mixing profile* that stabilizes spheres and in the previous case it is the *relative bending rigidity*.

The most obvious effect of changing the average composition for a homogenous sphere is that the bending rigidity (which is a constant) will vary. For a sphere consisting of mainly long chain molecules the bending rigidity is high, and this gives rise to low curvature, increasing the size of the sphere. However, if the sphere consists mainly of short chain molecules the bending rigidity is lower, giving rise to higher curvature which decreases the size of the sphere which has been observed (Baumgart, T., Hess, S. T., Webb, W. W. 2003). However, as mentioned before, our theory only considers constant area vesicles and thus cannot consider size variations of spherical vesicles. So at this point we cannot say how the composition varies for spherical vesicles.

An interesting result from the phase diagrams is that for a decrease in concentration, the stable state changes from the spherical vesicle to the oblate vesicle (figure 3.7-10).

This type of behavior is reported by experimenters (Nieh *et al.*, 2005) using small angle neutron scattering experiments (SANS) in which for low temperature ($T = 10°C$) oblate shaped vesicles exist (see section 1.7) and for higher concentration, polydisperse spherical vesicles exist. This experimental work even proposes that the composition profile of these oblates consist of long chain molecules in the low curvature region and short chain molecules in the high curvature region but this has not been verified by direct measurement. The composition profiles that we obtain also are similar to what Nieh *et al.* proposes.

3.4   Conclusion to Chapter 3

In this chapter we have examined axisymmetric ellipsoidal vesicles with constant area by modifying the theory of Julicher and Lipowsky to include varying degees of mixing such that the relative composition is coupled to the curvature. Our system exhibits phase transitions between oblates and spheres below the critical temperature. The relative bending rigidities and spontaneous curvature are found to have a predictable effect on the shape, thus the curvature variations of the vesicle. Some of the behavior exhibited is similar to that observed in experiments such as the oblate to sphere transition, the presence of segregated domains, and the correlation of long chains to low curvature regions and short chains to high curvature regions.

Appendix to Chapter 3

Conservation of Total Area of a Vesicle

In chapter three, calculations are done for vesicles with constant surface area. This constraint is imposed to mimic the tendency of lipid membranes to resist stretching which was mentioned in section 2.3.1. We need a formula for the length of the horizontal axis, a, that satisfies this. In order to implement this in terms of the geometric variables, θ and ε, given in the appendix to chapter two we will introduce a *reference vesicle*. This reference vesicle is a sphere ($\varepsilon = 1$) of radius $a = 1$. The total area of the vesicle will then be

$$A_{ref} = 4\pi a^2 = 4\pi \tag{3.A.1}$$

We use the area of an ellipsoid as given by (2.B.3):

$$A = 2\pi a^2 \int_0^\pi d\theta \sin\theta \sqrt{\cos^2\theta + \varepsilon^2 \sin^2\theta} \tag{3.A.1}$$

where a is the length of the horizontal axis. For a given ε, the value of a that conserves the area, A, to that of A_{ref} is found by setting

$$A = A_{ref} = 4\pi \tag{3.A.2}$$

By substituting this to the area of the ellipsoid and rearranging, we get the following equation for a:

$$\tag{3.A.3}$$

$$a = \frac{\sqrt{2}}{\left[\int_0^\pi d\theta \sin\theta \sqrt{\cos^2\theta + \varepsilon^2 \sin^2\theta} \right]^{1/2}}$$

so we now have an equation for a in terms of the eccentricity $(a = a(\varepsilon))$. This formula is

used for a in the free energy of mixing given in equation 2.B.6 and is solved numerically.

4. RESULTS FOR BILAYERED MICELLE TO VESICLE TRANSITION

4.1 Introduction

In this chapter we construct phase diagrams for vesicle to bicelle (or bicelle) transitions in the T vs u plane and in the T vs ϕ_{av} plane. Even though the vesicle and bicelle are described by the same free energies are the same (see equations 2.41-43), the two systems differ in structure. The bicelle is flat with zero curvature energy in the absence of spontaneous curvature, but has a positive edge energy proportional to λ. The vesicle has a positive curvature energy, but no edge energy. To find the thermodynamic range of stability of each phase we simply compare the bicelle energies to the stable vesicle energies at different values of (T, u). We study the effect of independent variations of the edge energy, λ, and spontaneous curvature, c_0, but not the bending rigidity, κ, or the coupling, J.

We do not obtain composition profiles for the bicelle. The bilayer region including the edge is assumed to be homogenous, in composition, while the edge energy is simply described by the parameter λ and the bilayer composition, ϕ. This means that the bicelle discussed here most closely resembles the mixed bicelle proposed by Triba *et al.* (2005)

4.2. Results and Discussion

Some phase diagrams in the T vs u plane are given in figures 4.1a-b. Vesicles have their own particular phase behavior, discussed in chapter 3, and we include this with the vesicle-bicelle phase diagram. A general feature of these graphs is that for low values of average composition (high amount of short chain molecules) the bicelle (labeled "D" in the diagrams) is more stable than the vesicle. At high temperatures we often see that the

two boundaries of the coexistence region cross each other so there is a low temperature

and high temperature coexistence region. The region where the two phase boundaries

cross is hard to understand as it is not a common phenomenon so we will not discuss it at

length.

In the coexistence region the average composition of oblates and bicelles are that

which correspond to points on the phase boundaries. The high-temperature D+O

boundary on the left is sometimes close to $\phi_{av} = 0$ and may even be indistinguishable

from the T axis. For such regions, the bicelle cannot be stable since there are not enough

long chain molecules to stabilize the bilayer. In fact at $\phi_{av} > 0$, mixed micelles will tend

to form and this is depicted in Triba et $al.$'s phase diagram in figure 1.11. Though, the

structure of these micelles is unknown.
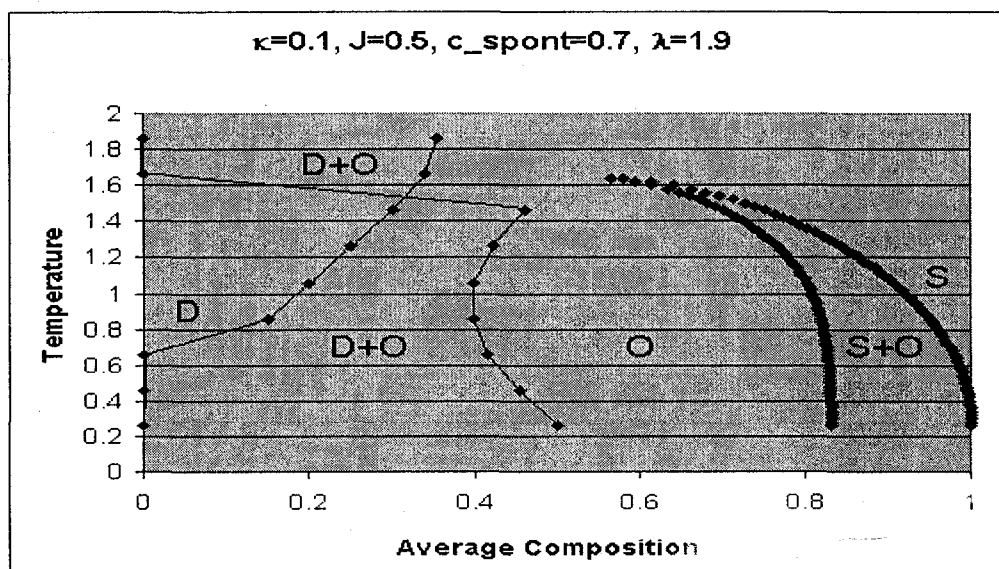
*Figure 4.1*

Figure 4.1-4. Temperature vs average composition (T vs ϕ_{av}) phase diagrams for bicelles or " disks" of varying edge energy, λ (fig 4.1., 4.2.) and varying spontaneous curvature, denoted "c_spont" (fig4.3. , 4.4.). Vesicle phases are denoted by S (sphere) and O (oblate) and their phase behavior is discussed in chapter 3. Disk phases are denoted by D. The transition occurs in the low composition regions of the diagram and exhibits a coexistence region, denoted by D+O.
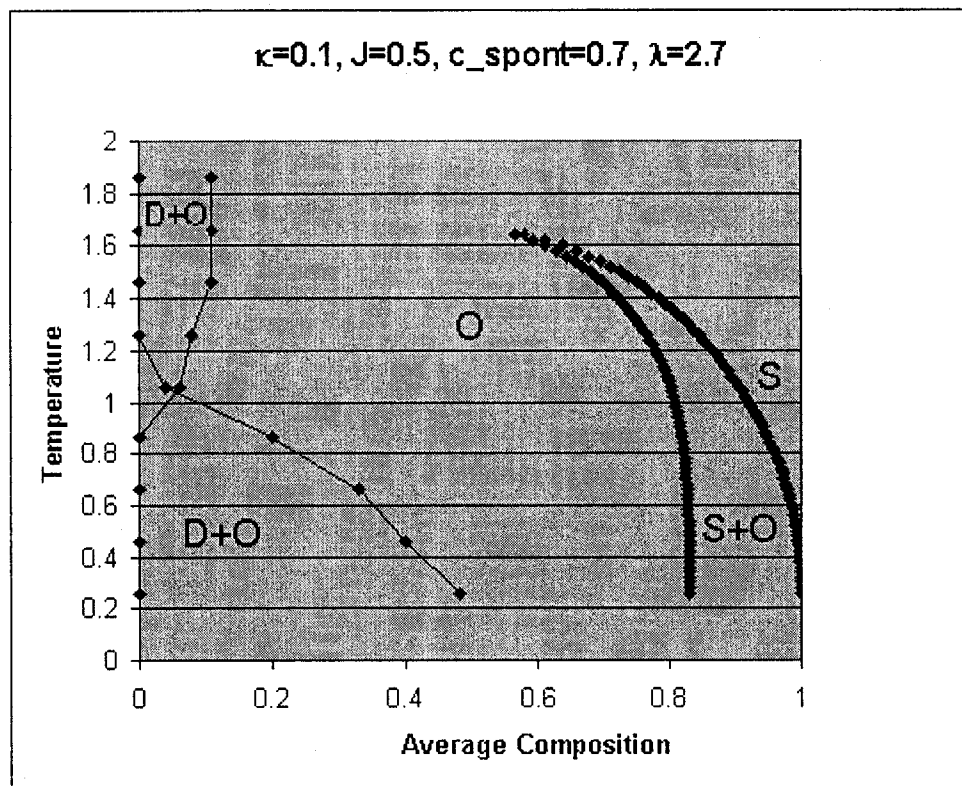
Figure 4.2. Caption below 4.1.
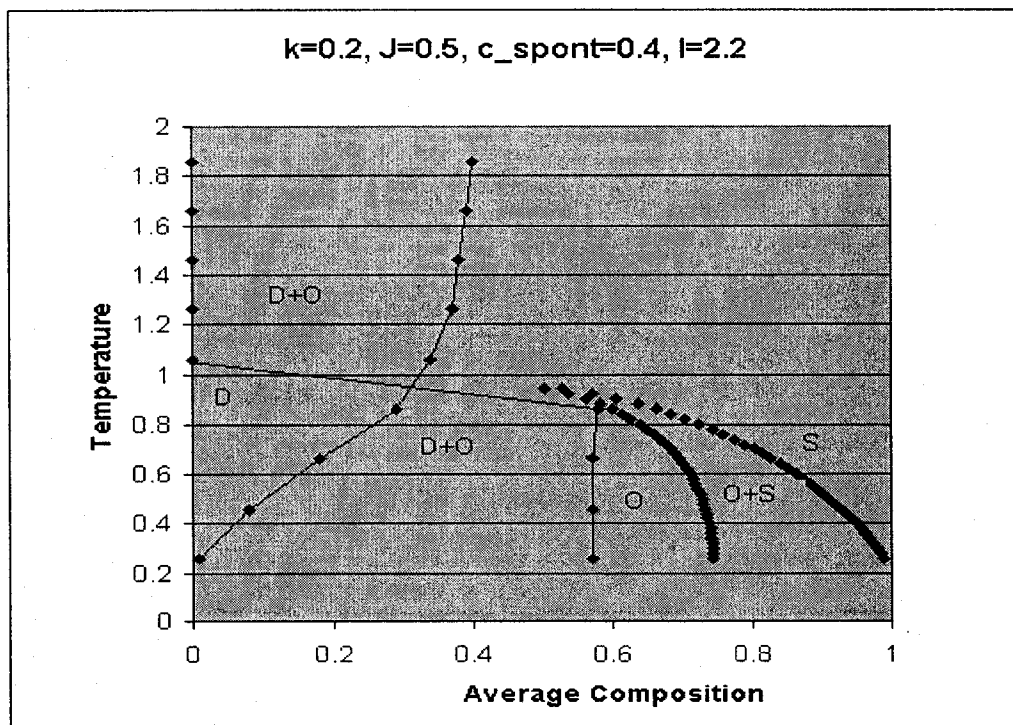
Figure 4.3. Caption below 4.2.
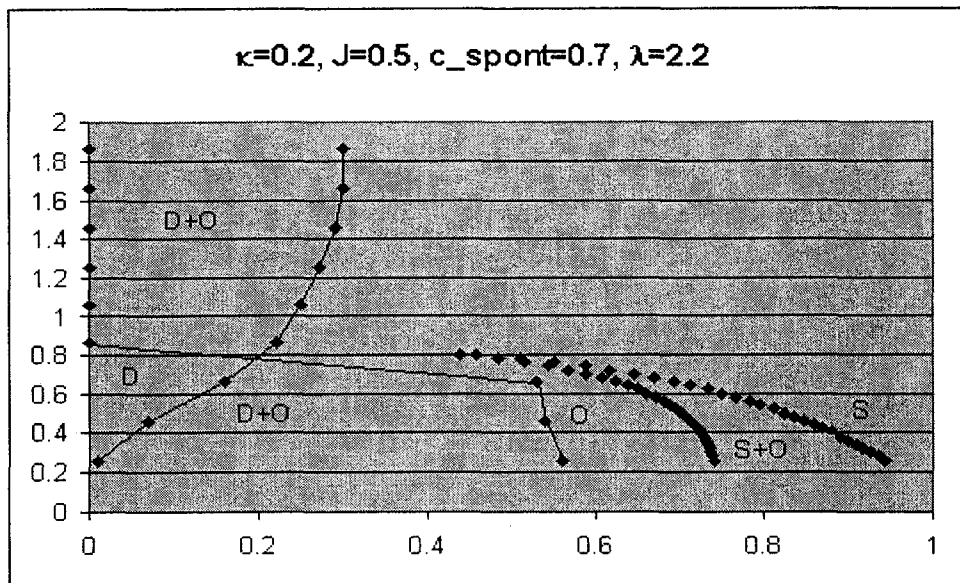
Figure 4.4. Caption below 4.1.

In figures 4.1 and 4.2, the bending rigidity, κ, the coupling, J and the spontaneous

curvature, c_0, are fixed while the edge energy is increased. We examine intermediate

values of λ because at low values of λ ($\kappa = 0.1$, $J = 0.5$ and $c_0 = 0.7$, for the case of λ δ

1.6), the phase boundaries cross at very low temperature. Increasing λ tends to shift both

phase boundaries to the left, decreasing the range of stability of the bicelle as depicted in

figures 4.1-2. The high temperature coexistence region decreases as well. λ represents

the unfavourable configuration of the edge region characteristic of bicelles so we expect

the bicelle to become less stable as λ increases.

In figures 4.3 and 4.4 the results of incr... ...g the spontaneous curvature while fixing

the other parameters are shown. In creasing c_0 generally decreases the region of stability

for the bicelle. In the case of $\kappa = 0.2$, $J = 0.5$ and $\lambda = 2.2$, the right phase boundary at

high temperature skips from $\phi_{av} > 0$ to $\phi_{av} > 1$ as c_0 is lowered past ~0.331. The bilayer

of the bicelle, by construction, has zero curvature and thus its bending energy is

proportional to c_0^2. So unless c_0 is zero, the bilayer is in an unfavourable configuration

and increasing the spontaneous curvature will tend to destabilize the bicelle. However the vesicle bilayer is allowed to bend and will tend to conform to curvature preferences.

The vesicle-bicelle phase diagram proposed by Triba *et al.* from NMR experiments is shown in figure 1.11 and in many respects is consistent with our results. In the experiments there are pure bicelle regions, pure vesicle regions and coexistence regions. The system studied by Triba *et al.* exhibits bicelles occuring at low temperatures for all degrees of short and long chain mixing as does Nieh *et al.* (2001) using small angle neutron scattering (SANS). Other systems explored by SANS show that bicelles occur at low temperatures but are replaced by vesicles if the fraction of long chain DMPC is high enough (Nieh *et al.*, 2005). Our phase diagrams are more consistent with the latter showing a bicelle-vesicle coexistence occurring between about at low values of ϕ_{av} for minimal values of the temperature. One problem with our result is the coexistence region for these low temperatures, which is not present in Nieh *et al.* (2005) and located at the high ϕ_{av} region in figure 1.11. However the experiments generally show that bicelles tend to exist at low temperature and our diagram does behave like this.

Another feature of our diagrams is the high temperature coexistence region. A high temperature coexistence region is observed by Triba *et al.* but has not been mentioned by the aforementioned SANS reports by Nieh *et al.* (2001, 2005). In figure 1.11 this coexistence region lies beside a high temperature, high ϕ_{av} region where multilamellar vesicles, MLV's, (see figure 4.5) reside (labeled V_m). Triba *et al.* suggest that the coexistence region precedes V_m where, as the fraction of long chain molecules increases, the bicelles join to form
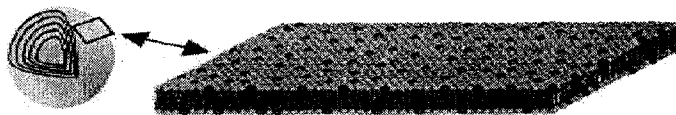
Figure 4.5. Multilamellar vesicle(left). A patch of a single lamellar layer (left). Taken from Triba et al.(2005).

extended bilayers that close up form MLV's. Our theory does not account for MLV's but does consider the stability of bicelles and vesicles and thus can be applied to figure 1.11.

Finally our diagrams exhibit high ϕ_{av} regions consisting of pure vesicles and low ϕ_{av} regions consisting of pure bicelles. These regions are also present in figure 1.11. The region between the pure vesicle and bicelle phases in figure 1.11 is unmeasured (indicated by the broken line) so it is unclear in this system the nature of the transition between the two phases. However in our diagram, we have a point where the two coexistence boundaries cross which, as mentioned earlier in the section, is an unusual phase behavior. However it is not inconsistent with the D+O phase boundary of Fig. 1.11 and it is possible that further experiments will find such behaviour in bicelle-vesicle systems.

4.3 Conclusion to Chapter 4

In this chapter we have examined the stability of the mixed bicelle and vesicle phases. Our model behaves such that increasing either the edge energy or spontaneous curvature destabilizes the bicelle in favour of the vesicle, which is expected in real systems. Our phase diagrams show behavior that is quite consistent with figure 1.11 and to some degree consistent with the results of Nieh et al. (2001; 2005). Finally our diagrams generally contain an unusual point where the two boundaries of the coexistence region cross that happens to be in the same vicinity as the unmeasured region of figure 1.11.

5. REFERENCES

Andersson, A. and Maler, L. 2006. Size and Shape of Fast-tumbling Bicelles as Determined by Translational Diffusion. *Langmuir.* 22, 2447.

Baumgart, T., Hess, S. T., Webb, W. W. 2003. Imaging coexisting fluid domains in biomembrane models coupling curvature and line tension. *Nature.* 425, 821.

Benton, W. J.1987. p207 *Physics of Amphiphilic Layers,* Vol. 21 of *Springer Proceedings in Physics* (Springer, Berlin)

Berndl, K., Kas, J., Lipowsky, R., Sackmann, E., Seifert, U. 1990. Shape Transformation of Giant Vesicles: Extreme Sensitivity to Bilayer Asymmetry. *Europhys. Lett.* 13, 659.

Boal, D. 2000. Size Limits of Very Small Organisms. *Space Studies Board, National Academy of Sciences.*

Boal, D. 2002a. p145-146 *Mechanics of the Cell,* (Cambridge University Press, New York)

Boal, D. 2002b. p141 *Mechanics of the Cell,* (Cambridge University Press, New York)

Boal, D. 2002c. p156 *Mechanics of the Cell,* (Cambridge University Press, New York)

Boal, D. 2002d. p158 *Mechanics of the Cell,* (Cambridge University Press, New York)

Chen, C-M., Higgs, P. G., MacKintosh, F. C. 1997. Theory of Fission for Two-Component Lipid Vesicles. *Physical Review Letters.* 79, 1579.

Duwe, H. P., Kaes, J. and Sackmann, E. 1990. Bending elastic moduli of lipid bilayers: modulation by solutes. *J. Phys. France.* 51, 945.

Faucon, F. F., Mitov, M. D., Melear, P., Bivas, I. and Bothorel, Pl 1989. Bending elasticity and thermal fluctuations of lipid membranes. Theoretical analysis and experimental requirements. *J. Phys. France.* 50, 2389

Hare, B. J., Prestegard, J. H., Engleman, D. M. 1995. Small angle X-ray Scattering Studies of Magnetically Oriented Lipid Bilayers. *Biophys. J.* 69, 1891.

Hu, J-G., Ou-Yang, Z-C. 1993. Shape Equations of the Axisymmetric Vesicles. *Physical Review E.* 47, 461.

Jones, R. A. L. 2002a. p147-148 *Soft Condensed Matter,* (Oxford University Press, New York)

Jones, R. A. L. 2002b. p145 *Soft Condensed Matter*, (Oxford University Press, New York)

Jones, R. A. L. 2002c. p149 *Soft Condensed Matter*, (Oxford University Press, New York)

Julicher, F. and Lipowski, R. 1993. Domain-Induced Budding of Vesicles. *Physical Review Letters.* 70, 2964.

Julicher, F. and Lipowski, R. 1996. Shape Transformations of Vesicles With Intramembrane Domains. *Physical Review E.* 53, 2670.

Katsaras, J., Donaberger, R. L., Swainson, I. P., Tennant, D. C., Tun, Z., Vold, R. R., Prosser, R. S. 1997. Rarely Observed Phase Transitions in a Novel Lyotropic Liquid Crystal System. *Physical Review Letters.* 78, 899.

Losonczi, J. A., Prestegard, J. H. 1998. Improved dilute bicelle solutions for high-resolution NMR of biological macro-molecules. *J Biomol. NMR.* 12, 447.

Meleard, P., Gerbeaud, C., Pott, T., Fernandez-Puente, L., Bivas, I., Mitov, M. D., Dufourcq, J. and Bothorel, P. 1997. Bending elasticities of model membranes: influences of tempera and sterol content. *Biophys. J.* 72, 2616.

Mutz, M. and Helfrich, W. 1990. Bending rigidities of some biological model membranes as obtained from the Fourier analysis of contour sections. *J. Phys. France.* 51, 991.

Nieh, M. P., Glinka, C. J., Kneger, S., Prosser, R. S. 2001. SANS Study of the Structural Phases of Magnetically Aligable Lanthanide-Doped Phospholipid Mixtures. *Langmuir.* 17, 2629.

Nieh, M. P., Glinka, C. J., Kruger, S., Prosser, R. S., Katsaras, J. 2002. SANS Study On the Effect of Lanthanide Ions and Charged Lipids on the Morphology of Phospholipid Mixtures. *Biophys. J.* 82, 2487.

Nieh, M-P. 2003. Concentration-Independent Spontaneously Forming Biomimetric Vesicles. *Physical Review Letters.* 91, 158105.

Nieh P-M. *et al.* 2005. Spontaneous Formed Unilamellar Vesicles with Path-Dependent Size Distribution. *Langmuir.* 21, 6656-6661.

Peliti, L. 1997a. p172 *Shapes and Fluctuations in Membranes*, a book chapter from *Physics ofBiological Systems*, (Springer, New York)

Peliti, L. 1997b. p173-176 *Shapes and Fluctuations in Membranes*, a book chapter from *Physics ofBiological Systems*, (Springer, New York)

Peliti, L. 1997c. p173 *Shapes and Fluctuations in Membranes*, a book chapter from *Physics ofBiological Systems*, (Springer, New York)

Raudino, A. 1995. Dynamics of Finite Size Lipid Bilayer. Narrowing of Bilayer Edge Induced by Its Nonlinear Elastic Properties. *J. Phys. Chem.* 99, 15298.

Safran, S. A. 1991. Stability and Phase Behavior of mixed surfactant vesicles. *Physical Review A.* 43, 1071.

Safran, S. A., 2003. *Statistical Thermodynamics of Surfaces, Interfaces and Membranes.* (Westview Press, Boulder, Colorado).

Sanders, C. R., Schwonek, J. P. 1992. Characterization of Magnetically Oriented Bilayers in Mixtures of Dihexanolphosphatidycholine and Dimyristoylphosphatidycholine by Solid State NMR. *Biochemistry.* 31, 8898.

Schneider, M. B., Jenkins, J. T. and Webb, W. W. 1984. Thermal fluctuations of large cylindrical phospholipid vesicles. *Biophys. J.* 45, 891.

Seifert, U. 1991. Vesicles of Toroidal Topology. *Physical Review Letters.* 66, 2404.

Seifert, U. 1993. Curvature-Induced Lateral Phase Segregation in Two-Component Vesicles. *Physical Review Letters.* 70, 1335.

Seifert, U., Berndl, K. and Lipowsky, R. 1991. Shape transformations of vesicles: Phase diagram for spontaneous- curvature and bilayer-coupling models. *Physical Review A.* 44, 1182.

Seifert and Lipowsky. 1995. *Morphology of Vesicles,* a chapter from *Handbook of Biological Physics.* (Elsevier, Amsterdam, 1999-2004)

Triba, M. N. *et al.* 2005. Reinvestigation by Phosphorus NMR of Lipid Distribution in Bicelles. *Biophysical Journal.* 88, 1887.

Veatch, S. L. and Keller S. L. 2005. Miscibility Phase Diagrams of Giant Vesicles Containing Sphingomyelin. *Physical Review Letters.* 94, 148101.